International Journal of Heat and Mass Transfer 219 (2024) 124847

Contents lists available at ScienceDirect

International Journal of Heat and Mass Transfer

journal homepage: www.elsevier.com/locate/ijhmt

Nonlinear thermal analysis of two-dimensional materials with memory

C.F. Munafò [a], P. Rogolino [a,*], R. Kovács [b,c]

[a] Department of Mathematics and Computer Sciences, Physical Sciences and Earth Sciences, University of Messina, Messina, Italy
[b] Department of Energy Engineering, Faculty of Mechanical Engineering, BME, Budapest, Hungary
[c] Department of Theoretical Physics, HUN-REN Wigner Research Centre for Physics, Institute for Particle and Nuclear Physics, Budapest, Hungary

ARTICLE INFO

Keywords:
Extended irreversible thermodynamics
Nonlinear heat transport
Non-Fourier heat conduction, finite differences, temperature dependent thermal conductivity

ABSTRACT

A nonlinear hyperbolic heat transport equation has been proposed based on the Cattaneo model without mechanical effects. We analyze the two-dimensional Maxwell-Cattaneo-Vernotte heat equation in a medium subjected to homogeneous and non-homogeneous boundary conditions and with thermal conductivity and relaxation time linearly dependent on temperature. Since these nonlinearities are essential from an experimental point of view, it is necessary to establish an effective and reliable way to solve the system of partial differential equations and study the behavior of temperature evolution. A numerical scheme of finite differences for the solution of the two-dimensional non-Fourier heat transfer equation is introduced and studied. We also investigate the attributes of the numerical method from the aspects of stability, dissipation and dispersive errors.

1. Introduction

In many industrial applications, most heat conduction problems are described and analyzed using Fourier's law. Although Fourier's heat equation applies to several engineering tasks, it also has some physical defects, such as the infinite thermal propagation speed. The classical Fourier law is no longer applicable when one is interested in the transient evolution of both heat flux and temperature fields for extremely short time intervals, nanoscale behavior, for low-temperature situations, or to describe the simultaneous presence of multiple heat transfer channels present, e.g., in a heterogeneous material.

Non-Fourier theories are of great interest and constitute a subject of intense research in the engineering field due to the use of heat sources in many applications such as metal melting [1], and functionally graded materials (FGMs) [2]. In these situations, Fourier's classical law is inappropriate. Thermal effects coupled with mechanical effects are present in the propagation of second sound in dielectric crystals at low-temperature [3–5]. Several authors have conducted research on NaF [6–8], for instance, Jackson et al., [4,9] detected heat waves in solid sodium fluoride (NaF) in the range of 12 K to 15 K, and from 13 K three peaks can be distinguished, longitudinal and transverse ballistic signals – thermo-mechanical waves – and second sound which can be interpreted as a damped temperature wave. Analogous experimental results have been obtained by Narayanamurti et al. [5] in Bismuth (Bi) in the range from 3 K to 5 K.

Similar heat pulse experiments have been carried out in recent decades under various circumstances. For instance, in [10], two experimental setups are used to observe effects beyond Fourier's law in a heterogeneous material structure. In [11], the non-Fourier type heat conduction experiment in heterogeneous materials (rocks) at room temperature is performed, and the authors have observed over-diffusion and, besides, the size-dependence of thermal parameters, even in Fourier's case. Heat waves have also been detected in a nanoscale process [12] since the nanoscale characteristic length allows the heat carriers to achieve any point of the system before the heat flux relaxes to its equilibrium value. Nowadays, high-frequency thermal waves cover a great interest in two-dimensional (2D) materials, especially in graphene due to their high intrinsic thermal conductivity and a long relaxation time of heat flux [13].

Under these circumstances, a modified constitutive model for the transport process, resulting in a finite speed of the thermal wave, is proposed by Cattaneo-Vernotte (CV) [14]. The hyperbolic heat conduction equation based on the CV model includes a relaxation mechanism to adapt to a change in temperature gradient gradually.

The thermal transport processes with finite velocity constitute an interesting theme also in continuum thermodynamics which, in previous decades, has led to a new investigation of the classical rational thermodynamics (RT) [15] and to the formulation of extended irreversible thermodynamics [16–18] and rational extended thermodynamics (RET) [19].

* Corresponding author.
E-mail addresses: carmelofilippo.munafo@unime.it (C.F. Munafò), patrizia.rogolino@unime.it (P. Rogolino), kovacs.robert@wigner.hu (R. Kovács).

https://doi.org/10.1016/j.ijheatmasstransfer.2023.124847
Received 27 July 2023; Received in revised form 4 October 2023; Accepted 17 October 2023
Available online 31 October 2023

In recent years, many authors have paid particular attention to using models beyond Fourier for low-temperature problems [20–27]. For instance, in [28], the consequences of a nonlinearity in second-sound phenomenon are modeled in a particular way, using a special case of the Cattaneo-Vernotte equation. In their approach, the relation between the relaxation time and the thermal conductivity is different than what we investigate here.

However, by virtue of the difficulties in the analytic investigation of systems with complicated geometries or boundary conditions, the interest in identifying suitable numerical schemes for analyzing such problems has been increased.

In a previous paper, [29], a nonlinear model for heat conduction considering the temperature dependence in thermodynamic parameters has been introduced. It has been shown that the second law of thermodynamics functionally connects thermal conductivity and relaxation time. Therefore, the temperature dependence of one parameter influences the other. Furthermore, an explicit forward difference scheme is applied to a one-dimensional problem, moreover, the main aspects of the numerical method and its stability properties are discussed both for the Fourier and the Cattaneo-Vernotte equations.

In the present paper, we further improve the previous approach for analyzing the nonlinear hyperbolic CV equation in two spatial dimensions, studying the influence of spatially homogeneous and non-homogeneous time-dependent boundary conditions. We provide insights about the boundary conditions, and how the temperature dependence can affect the measurable temperature history.

The structure of the paper is as follows. In Section 2, we deduce a nonlinear non-Fourier type model suggested by Cattaneo and Vernotte, analyzing the compatibility of the entropy principle on the constitutive relations of the rigid conductor subject to thermal processes. Then, in Section 3, the crucial aspects of the numerical scheme, its stability properties, and the accuracy of the method are discussed. In Section 4, we provide a numerical solution under suitable homogeneous and non-homogeneous boundaries and initial conditions. Finally, in Section 5, we discuss our results as well as possible future developments.

2. Nonlinear model of heat transfer

In classical thermodynamics, most of the heat conduction problems are described and analyzed by using Fourier's law that relates the heat flux $\mathbf{q}$ with the gradient of the local equilibrium temperature T:

$$\mathbf{q} = -\lambda \nabla T \tag{1}$$

where the coefficient λ represents the thermal conductivity for an isotropic material. To describe the evolution of temperature, the constitutive relation Eq. (1) is combined with the internal energy balance,

$$\rho \frac{\partial e}{\partial t} + \nabla \cdot \mathbf{q} = 0, \tag{2}$$

where ρ is the mass density, e is the specific internal energy, and $\nabla\cdot$ stands for divergence operator. We omit any internal volumetric heat sources, and consider a rigid material, thus we also neglect the mechanical contributions. The CV equation expresses the modified constitutive model:

$$\tau \frac{\partial \mathbf{q}}{\partial t} + \mathbf{q} = -\lambda \nabla T, \tag{3}$$

where τ is the relaxation time, and the time derivative term represents the presence of memory effects, i.e., the states in earlier time instants are also taken into account. It is also understood as inertia or lagging effect, especially in the framework of the dual-phase-lag concept. From a phonon hydrodynamic point of view, the increase of τ expresses the lower number of resistive collisions among phonons, the normal process takes place, and thus the wave nature of heat conduction becomes apparent.

The second law of thermodynamics represents a valuable tool for deriving the Fourier heat equation and generalizations of Fourier's law. In many cases, only linear relations between the thermodynamic fluxes and forces are considered. More specifically, we focus on temperature-dependent phenomenological coefficients and not on the role of nonlinear flux or force terms (such as $(\nabla T)^3$).

Indeed, the thermodynamic admissibility of thermal processes is guaranteed by the second law of thermodynamics, requiring non-negative entropy production. Locally, this requirement reads

$$\sigma_s = \rho \frac{\partial s}{\partial t} + \nabla \cdot \mathbf{J_s} \geq 0, \tag{4}$$

in which s and $\mathbf{J}_s$ are the specific entropy and the local entropy flux, respectively. In several papers [15,17,30], the compatibility with the second law of both models, (1) and (3), under the assumptions of constant material functions has been tested. In [29], we investigated a particular nonlinearity in which the thermal conductivity and the relaxation time are no longer constant but depend on the temperature linearly.

A constitutive theory requires the choice of the so-called state variables. Let us assume the state space is spanned by the variables $(e, \mathbf{q})$, [31], thus it is postulated the following form for the specific entropy:

$$s(e, \mathbf{q}) = s_{eq}(e) - \frac{m(e)}{2} \mathbf{q} \cdot \mathbf{q}, \tag{5}$$

where s_{eq} is the classical specific entropy representing the equilibrium entropy and $m(e)$ is a positive function. Taking into account the Gibbs relation, and the balance equation (2), after some rearrangements the entropy production reads:

$$-\rho m(e) \mathbf{q} \frac{\partial \mathbf{q}}{\partial t} - \frac{1}{2} \rho \frac{\partial m(e)}{\partial e} \frac{\partial e}{\partial t} \mathbf{q} \cdot \mathbf{q} + \mathbf{q} \cdot \nabla \frac{1}{T} \geq 0. \tag{6}$$

We limit ourselves to the case in which $\partial_e m(e) = 0$, hence $m(e) = m$ is a positive constant, thus one obtains:

$$\sigma_s = \left[-\rho m \partial_t \mathbf{q} + \nabla \left(\frac{1}{T} \right) \right] \cdot \mathbf{q} \geq 0. \tag{7}$$

Following Onsager's procedure [32], a relationship between the thermodynamic fluxes and forces is provided:

$$-\rho m \frac{\partial \mathbf{q}}{\partial t} + \nabla \left(\frac{1}{T} \right) = l \mathbf{q}, \tag{8}$$

where the phenomenological coefficients m and l are positive functions. The following identifications

$$\tau_R = \frac{\rho m}{l}, \qquad \lambda_T = \frac{1}{l T^2} \tag{9}$$

lead to the nonlinear CV heat equation

$$\tau_R(T) \frac{\partial \mathbf{q}}{\partial t} + \mathbf{q} = -\lambda_T(T) \nabla T. \tag{10}$$

We wish to note again that this evolution equation, and the relation between τ and λ are the consequence of the flux-force relation (8). A compatible, but different setting is studied in [28], and further possibilities can exist. Let us consider a rigid heat conductor, and we suppose that the thermal conductivity and relaxation time are linearly related to the temperature as follows:

$$\lambda_T(T) = \lambda_0 + a(T - T_0) \tag{11a}$$

$$\tau_R(T) = \tau_0 + b(T - T_0) \tag{11b}$$

where λ_0, τ_0 are the thermal conductivity and the relaxation time at the initial (or reference) temperature, respectively, a and b are the coefficients that depend on the material and could be both positive and negative, which, if they are not zero determine the nonlinearity of the material parameters.

After taking into account the identifications (9), in order to get these linear expressions for λ_T and τ_R, (11a) and (11b), the following constraints arise, [29]:

$$l(T) = \frac{1}{\left[\lambda_0 + a(T - T_0)\right] T^2}, \quad \rho m = \frac{\tau_0 + b(T - T_0)}{\left[\lambda_0 + a(T - T_0)\right] T^2}. \tag{12}$$

Since m is a constant, it is necessary to consider a temperature-dependent mass density ($\rho = \rho(T)$) that refers to the presence of mechanical effects. Therefore, while it would contradict our basic assumption of dealing with rigid material, we still find it necessary to study that particular subsystem without mechanics. We wish to focus on the characteristics of temperature evolution and the properties of the solution method with respect to its stability and dispersion error. Thus we analyze the nonlinear CV heat equation in the hypothesis in which the mass density ρ remains constant.

2.1. Two-dimensional formulation

Let us consider the set of equations (2) and (10) in a two-dimensional rectangular domain $\Omega = [0, L_1] \times [0, L_2]$ with lengths of L_1 and L_2,

$$\rho(T)c\,\frac{\partial T}{\partial t} + \frac{\partial q_x}{\partial x} + \frac{\partial q_y}{\partial y} = 0, \tag{13a}$$

$$\tau_R(T)\frac{\partial q_x}{\partial t} + q_x = -\lambda_T(T)\frac{\partial T}{\partial x}, \tag{13b}$$

$$\tau_R(T)\frac{\partial q_y}{\partial t} + q_y = -\lambda_T(T)\frac{\partial T}{\partial y}, \tag{13c}$$

where c is the specific heat, $e = cT$, and q_x, q_y are the components of the heat flux $\mathbf{q} = (q_x, q_y)$. The specific heat capacity c is assumed to be constant. Initially, in a heat pulse experiment, it is required to have homogeneous temperature distribution and that the sample is in thermal equilibrium with its environment. Thus both heat flux fields are zero at the initial time instant. Regarding the boundary conditions, the heat pulse excites the lower side of the sample in the y-axis direction, the other sides of the domain are considered to be adiabatic. Hence, we assign the following initial conditions,

$$T(x, y, 0) = T_0, \qquad q_x(x, y, 0) = 0, \qquad q_y(x, y, 0) = 0, \tag{14}$$

and boundary conditions only for heat flux field,

$$q_x(0, y, t) = 0, \quad q_x(L_1, y, t) = 0, \quad q_y(x, 0, t) = 0. \tag{15}$$

Subsequently, on one of its sides, is applied a homogeneous heat flux

$$q_y(x, L_2, t) = q_y^0(t) = \begin{cases} \dfrac{q_{max}}{2}\left[1 - \cos\left(\dfrac{2\pi t}{t_p}\right)\right] & \text{if } 0 < t \le t_p, \\ 0 & \text{if } t > t_p, \end{cases} \tag{16}$$

or a spatially non-homogeneous one

$$q_y(x, L_2, t) = q_y^0(t) = \begin{cases} \dfrac{q_{max}}{4}\left[1 - \cos\left(\dfrac{2\pi t}{t_p}\right)\right] \cdot \left[1 - \cos\left(\dfrac{2\pi x}{w_x}\right)\right] & \text{if } 0 < t \le t_p, \\ & \text{and} \\ & \frac{L_1 - w_x}{2} \le x \le \frac{L_1 + w_x}{2} \\ 0 & \text{if } t > t_p, \end{cases} \tag{17}$$

where t_p is the duration of the pulse, q_{max} is its amplitude, w_x is its spatial width.

The system (13a)-(13c) may contain coefficients with several orders of magnitude difference, this is unfavorable from a numerical point of view. Thus it is convenient to introduce dimensionless variables,

$$\hat{x} = \frac{x}{L_1}, \quad \hat{y} = \frac{y}{L_2}, \quad \hat{t} = \frac{\alpha_0 t}{L_1 L_2}, \quad \hat{q}_x = \frac{q_x}{\tilde{q}_0}, \quad \hat{q}_y = \frac{q_y}{\tilde{q}_0}, \quad \hat{T} = \frac{T - T_0}{T_{end} - T_0}, \tag{18}$$

where

$$\alpha_0 = \frac{\lambda_T(T_0)}{\rho_0 c}, \qquad T_{end} = T_0 + \frac{t_p \tilde{q}_0}{\rho_0 c L_2}, \qquad \rho_0 = \rho(T_0)$$

with

$$\tilde{q}_0 = \frac{q_{max}}{2} \qquad \text{for spatially homogeneous boundary heat flux,} \qquad \text{or}$$

$$\tilde{q}_0 = \frac{q_{max}}{4} \qquad \text{for spatially hon-homogeneous boundary heat flux,}$$

and thus, the dimensionless parameters are

$$\tau_{p_1}^{q_x} = \frac{\alpha_0 t_p}{L_1 L_2} = \tau_d, \quad \tau_{p_1}^{q_y} = \frac{\alpha_0 t_p}{(L_2)^2}, \quad \tau_{p_2}^{q_x} = \frac{a(T_{end} - T_0)t_p}{\rho_0 c L_1 L_2},$$
$$\tau_{p_2}^{q_y} = \frac{a(T_{end} - T_0)t_p}{\rho_0 c (L_2)^2}, \tau_{q_1} = \frac{\alpha_0 \tau_0}{L_1 L_2}, \quad \tau_{q_2} = \frac{\alpha_0\, b(T_{end} - T_0)}{L_1 L_2}, \quad \tau_d = \frac{\alpha_0 t_p}{L_1 L_2}.$$

Under these assumptions, the two-dimensional version of the dimensionless system of equations becomes:

$$\tau_d\left(1 + \frac{\tau_{q_2}}{\tau_{q_1}}\hat{T}\right)\frac{\partial \hat{T}}{\partial \hat{t}} + \frac{L_2}{L_1}\frac{\partial \hat{q}_x}{\partial \hat{x}} + \frac{\partial \hat{q}_y}{\partial \hat{y}} = 0, \tag{19a}$$

$$\left(\tau_{q_1} + \tau_{q_2}\hat{T}\right)\frac{\partial \hat{q}_x}{\partial \hat{t}} = -\hat{q}_x - \left(\tau_{p_1}^{q_x} + \tau_{p_2}^{q_x}\hat{T}\right)\frac{\partial \hat{T}}{\partial \hat{x}}, \tag{19b}$$

$$\left(\tau_{q_1} + \tau_{q_2}\hat{T}\right)\frac{\partial \hat{q}_y}{\partial \hat{t}} = -\hat{q}_y - \left(\tau_{p_1}^{q_y} + \tau_{p_2}^{q_y}\hat{T}\right)\frac{\partial \hat{T}}{\partial \hat{y}}, \tag{19c}$$

in which, from now on, the 'hat' is omitted in order to simplify the notation.
Furthermore, the dimensionless initial data are given:

$$\hat{T}(\hat{x}, \hat{y}, 0) = 0, \qquad \hat{q}_x(\hat{x}, \hat{y}, 0) = 0, \qquad \hat{q}_y(\hat{x}, \hat{y}, 0) = 0, \tag{20}$$

and the dimensionless form of boundary conditions for heat flux with the heat pulse with t_p duration read:

$$\hat{q}_x(0, \hat{y}, \hat{t}) = 0, \quad \hat{q}_x(1, \hat{y}, \hat{t}) = 0, \quad \hat{q}_y(\hat{x}, 0, \hat{t}) = 0. \tag{21}$$

Additionally, the heat pulse in the homogeneous case is

$$\hat{q}_y(\hat{x}, 1, \hat{t}) = \begin{cases} 1 - \cos\left(\dfrac{2\pi \hat{t}}{\tau_d}\right) & \text{if } 0 < \hat{t} \le \tau_d, \\ 0 & \text{if } \hat{t} > \tau_d. \end{cases}, \tag{22}$$

and in the non-homogeneous situation it reads

$$\hat{q}_y(\hat{x}, 1, \hat{t}) = \begin{cases} \left[1 - \cos\left(\dfrac{2\pi \hat{t}}{\tau_d}\right)\right] \cdot [1 - \cos(2\pi\hat{x})] & \text{if } 0 < \hat{t} \le \tau_d, \\ & \text{and } 0 \le \hat{x} \le 1 \\ 0 & \text{if } \hat{t} > \tau_d. \end{cases} \tag{23}$$

Remark 1. If we choose $\tau_{q_2} = \tau_{p_2}^{q_x} = \tau_{p_2}^{q_y} = 0$, it yields the linear case:

$$\tau_d\frac{\partial \hat{T}}{\partial \hat{t}} + \frac{L_2}{L_1}\frac{\partial \hat{q}_x}{\partial \hat{x}} + \frac{\partial \hat{q}_y}{\partial \hat{y}} = 0, \tag{24a}$$

$$\tau_{q_1}\frac{\partial \hat{q}_x}{\partial \hat{t}} = -\hat{q}_x - \tau_{p_1}^{q_x}\frac{\partial \hat{T}}{\partial \hat{x}}, \tag{24b}$$

$$\tau_{q_1}\frac{\partial \hat{q}_y}{\partial \hat{t}} = -\hat{q}_y - \tau_{p_1}^{q_y}\frac{\partial \hat{T}}{\partial \hat{y}}. \tag{24c}$$

As in [33,34], we apply a numerical scheme to solve the system (19a)-(19c) with a staggered field discretization for spatial derivatives in which the specific extensive quantities are calculated at the center of the cells. At the same time, the boundary-related fluxes are computed on the cell boundary, as we can see in the next section.

As a result, the spatial positions of the temperature values are shifted by a half space step from the positions of the $\mathbf{q}$ values (see Fig. 1).

3. Numerical framework

This section presents a numerical method developed for the nonlinear two-dimensions model (19a)(19c). Let us discretize the spatial

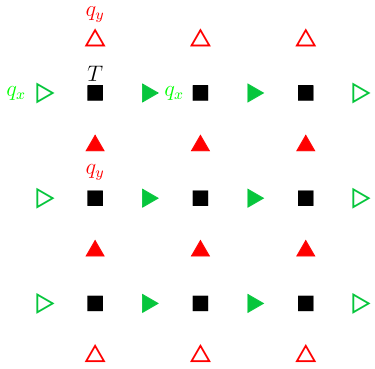

Fig. 1. Representation of the finite difference numerical scheme. The filled squares represent the temperature, and the filled triangles, which are oriented differently, are vector components. Empty symbols denote boundary conditions.

domain $\Omega = [0, L_1] \times [0, L_2]$ with spatial steps $\Delta x, \Delta y$ and the time interval $[0, t_{max}]$ with step Δt, the following discrete space and time values are obtained

$$x_j = x_0 + j\Delta x \quad j = 0, 1, 2, ..., N \tag{25a}$$

$$y_i = y_0 + i\Delta y \quad i = 0, 1, 2, ..., M \tag{25b}$$

$$t^n = n\Delta t \quad n = 0, 1, 2, ..., J. \tag{25c}$$

An explicit forward finite difference method is used for the time derivatives

$$\frac{\partial T}{\partial t} \simeq \frac{T^{n+1}_{i+1/2,j+1/2} - T^n_{i+1/2,j+1/2}}{\Delta t}, \tag{26a}$$

$$\frac{\partial q_x}{\partial t} \simeq \frac{(q_x)^{n+1}_{i+1/2,j} - (q_x)^n_{i+1/2,j}}{\Delta t}, \tag{26b}$$

$$\frac{\partial q_y}{\partial t} \simeq \frac{(q_y)^{n+1}_{i,j+1/2} - (q_y)_{i,j+1/2}}{\Delta t}, \tag{26c}$$

and for the spatial derivatives

$$\frac{\partial q_x}{\partial x} \simeq \frac{(q_x)^n_{i+1/2,j+1} - (q_x)^n_{i+1/2,j}}{\Delta x} = \mathcal{D}_x(q_x), \tag{27a}$$

$$\frac{\partial q_y}{\partial y} \simeq \frac{(q_y)^n_{i+1,j+1/2} - (q_y)^n_{i,j+1/2}}{\Delta y} = \mathcal{D}_y(q_y), \tag{27b}$$

$$\frac{\partial T}{\partial x} \simeq \frac{T^n_{i+1/2,j+1/2} - T^n_{i+1/2,j-1/2}}{\Delta x} = \mathcal{D}_x(T), \tag{27c}$$

$$\frac{\partial T}{\partial y} \simeq \frac{T^n_{i+1/2,j+1/2} - T^n_{i-1/2,j+1/2}}{\Delta y} = \mathcal{D}_y(T). \tag{27d}$$

In addition, for nonlinear terms, the following identifications are given

$$\left(\tau_{q_1} + \tau_{q_2} T\right) \simeq \left(\tau_{q_1} + \tau_{q_2} T^n_{i+1/2,j+1/2}\right) = \mathcal{A} \tag{28a}$$

$$\left(\tau^{q_x}_{p_1} + \tau^{q_x}_{p_2} T\right) \simeq \left(\tau^{q_x}_{p_1} + \tau^{q_x}_{p_2} T^n_{i+1/2,j+1/2}\right) = \mathcal{B}_x \tag{28b}$$

$$\left(\tau^{q_y}_{p_1} + \tau^{q_y}_{p_2} T\right) \simeq \left(\tau^{q_y}_{p_1} + \tau^{q_y}_{p_2} T^n_{i+1/2,j+1/2}\right) = \mathcal{B}_y \tag{28c}$$

As a result, the difference equations consist of an explicit forward differencing scheme

$$\mathcal{A}\frac{\tau_d}{\tau_{q_1}} \frac{T^{n+1}_{i+1/2,j+1/2} - T^n_{i+1/2,j+1/2}}{\Delta t} + \frac{L_2}{L_1}\mathcal{D}_x(q_x) + \mathcal{D}_y = 0, \tag{29a}$$

$$\mathcal{A}\frac{(q_x)^{n+1}_{i+1/2,j} - (q_x)^n_{i+1/2,j}}{\Delta t} = -(q_x)^n_{i+1/2,j} - \mathcal{B}_x\,\mathcal{D}_x(T), \tag{29b}$$

$$\mathcal{A}\frac{(q_y)^{n+1}_{i,j+1/2} - (q_y)_{i,j+1/2}}{\Delta t} = -(q_y)^n_{i,j+1/2} - \mathcal{B}_y\,\mathcal{D}_y(T), \tag{29c}$$

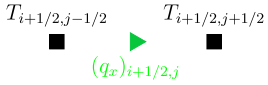

Fig. 2. Concept of the discretization for the first component of heat flux q_x.

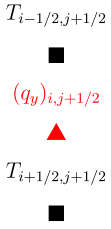

Fig. 3. Concept of the discretization for heat flux component q_y.

Accordingly, the discrete values of temperature are shifted in x and y directions

$$T^n_{i+1/2,j+1/2} \qquad \text{at} \qquad t^n,\ x_{j+1/2},\ y_{i+1/2}$$

and the heat flux components are only shifted in the direction corresponding to their Cartesian index, i.e. q_y in the x direction while q_x in the y direction (see Fig. 1):

$$(q_x)^n_{i+1/2,j} \qquad \text{at} \qquad t^n,\ x_j,\ y_{i+1/2},$$

$$(q_y)^n_{i,j+1/2} \qquad \text{at} \qquad t^n,\ x_{j+1/2},\ y_i.$$

Hence, the temperature is computed [29,35] in the internal nodes. The two components of heat flux, q_x and q_y, are shifted by half space step $\Delta x/2$ and $\Delta y/2$ respectively, as it is shown in Fig. 1. Furthermore, no boundary conditions will be prescribed for temperature as it can be expressed explicitly, like function of the earlier quantities. By virtue of the evolution equation of the heat flux component q_x, (29b), the term $T^n_{i+1/2,j+1/2}$ is replaced by the following average:

$$T^n_{i+1/2,j+1/2} \longmapsto \frac{T^n_{i+1/2,j-1/2} + T^n_{i+1/2,j+1/2}}{2}, \tag{30}$$

as shown in the Fig. 2.

By equation (29c), the term $T^n_{i+1/2,j+1/2}$ is replaced by the following average:

$$T^n_{i+1/2,j+1/2} \longmapsto \frac{T^n_{i-1/2,j+1/2} + T^n_{i+1/2,j+1/2}}{2}, \tag{31}$$

as shown in the Fig. 3.

3.1. Stability analysis

Due to the fact that a finite difference scheme can lead to instability, a stability analysis is recommended in order to investigate the region of the appropriate values of Δx, Δy and Δt for the given scheme. To study the stability of the assigned numerical scheme (29a)-(29c) the Von-Neumann procedure is used, then suppose that the solutions of the difference equations are in the following form [36]:

$$u^n_{l,j} = u_0\,\xi^n e^{i\,k_x\,j\Delta x} e^{i\,k_y\,l\Delta y} \tag{32}$$

with $u \in \{T, q_x, q_y\}$, i is the imaginary unit, k_x and k_y the wave numbers, and ξ is the growth factor representing the amplitude wave and must be bounded from above for stability.

Substituting the equation (32) into the difference equations, the system of linear algebraic equations is achieved:

$$\mathbf{M} \cdot (T_0,\, q_{x(0)},\, q_{y(0)})^T = 0 \tag{33}$$

wherein the coefficient matrix is:

$$\mathbf{M}=\begin{pmatrix} \frac{\tau_d}{\Delta t}\left(1+\frac{\tau_{q_2}}{\tau_{q_1}}Z\right)(\xi-1) & \frac{1}{\hat{L}\Delta x}\left(e^{ik_x\Delta x}-1\right) & \frac{1}{\Delta y}\left(e^{ik_y\Delta y}-1\right) \\ \frac{\tau_{p_1}^{q_x}+\tau_{p_2}^{q_x}Z}{\Delta x}\left(1-e^{-ik_x\Delta x}\right) & 1+\frac{\tau_{q_1}+\tau_{q_2}Z}{\Delta t}(\xi-1) & 0 \\ \frac{\tau_{p_1}^{q_y}+\tau_{p2}^{q_y}Z}{\Delta y}\left(1-e^{-ik_y\Delta y}\right) & 0 & 1+\frac{\tau_{q_1}+\tau_{q_2}Z}{\Delta t}(\xi-1) \end{pmatrix},$$

with $Z=\max_{i,j,n}T_{ij}^n$ and $\hat{L}=\dfrac{L_2}{L_1}$.

Remark 2. It is worth noting that the above numerical method is developed for linear heat equations. Since a nonlinearity appears in the right hand side of the resulting finite difference equations (29a)-(29c), one could assume apriori the maximum temperature and apply a linear stability analysis by following von Neumann's method [36] and Jury conditions [37]. In the Appendix B, we also investigated the stability of the present scheme in a one-dimensional situation. We admit that it highly relies on the initial assumption of the maximum temperature. To partially overcome this difficult, for a first estimation, one can execute a linear simulation and observe the maximum value of the resulting temperature field. This value can serve as a good estimate as the practically relevant nonlinearities do not increase the temperature remarkably, instead, they more notably distort the history.

The characteristic equation for ξ ($\det\mathbf{M}=0$) can be expressed as

$$p(\xi)=a_3\xi^3+a_2\xi^2+a_1\xi+a_0=0, \tag{34}$$

in which the coefficients are

$$a_3=\frac{\tau_d(\tau_{q_1}+\tau_{q_2}Z)^3}{\tau_{q_1}(\Delta t)^3}, \tag{35a}$$

$$a_2=-3\frac{\tau_d(\tau_{q_1}+\tau_{q_2}Z)^3}{\tau_{q_1}(\Delta t)^3}+2\frac{\tau_d(\tau_{q_1}+\tau_{q_2}Z)^2}{\tau_{q_1}(\Delta t)^2}, \tag{35b}$$

$$a_1=3\frac{\tau_d(\tau_{q_1}+\tau_{q_2}Z)^3}{\tau_{q_1}(\Delta t)^3}-4\frac{\tau_d(\tau_{q_1}+\tau_{q_2}Z)^2}{\tau_{q_1}(\Delta t)^2}+\frac{\tau_{q_1}+\tau_{q_2}Z}{\Delta t}\left(\frac{\tau_d}{\tau_{q_1}}-\Gamma\right), \tag{35c}$$

$$a_0=-\frac{\tau_d(\tau_{q_1}+\tau_{q_2}Z)^3}{\tau_{q_1}(\Delta t)^3}+2\frac{\tau_d(\tau_{q_1}+\tau_{q_2}Z)^2}{\tau_{q_1}(\Delta t)^2}-\frac{\tau_{q_1}+\tau_{q_2}Z}{\Delta t}\left(\frac{\tau_d}{\tau_{q_1}}-\Gamma\right)-\Gamma, \tag{35d}$$

$$\Gamma=\frac{\tau_{p_1}^{q_y}+\tau_{p_2}^{q_y}Z}{(\Delta y)^2}\left[\cos(k_y\Delta_y)-1\right]+\frac{\tau_{p_1}^{q_x}+\tau_{p_2}^{q_x}Z}{\hat{L}(\Delta x)^2}\left[\cos(k_x\Delta_x)-1\right] \tag{35e}$$

$$=-2S_2^2\frac{\tau_{p_1}^{q_y}+\tau_{p_2}^{q_y}Z}{(\Delta y)^2}-2S_1^2\frac{\tau_{p_1}^{q_x}+\tau_{p_2}^{q_x}Z}{\hat{L}(\Delta x)^2}\le 0,$$

with $S_1=\sin(k_x\Delta x/2)$, $S_2=\sin(k_y\Delta y/2)$.

Theorem 1. *The numerical scheme (29a)-(29c) is stable if the following conditions are satisfied*

1. *if* $\Gamma\le-\dfrac{\tau_d}{4\tau_{q_1}}$ *then* $0<\Delta t<-\dfrac{\tau_d(\tau_{q_1}+\tau_{q_2}Z)}{2\tau_{q_1}\Gamma}$,
2. *if* $-\dfrac{\tau_d}{4\tau_{q_1}}<\Gamma<0$ *then* $0<\Delta t<2(\tau_{q_1}+\tau_{q_2}Z)$.

Proof. In order to prove this result, we apply the Jury criterion [37]. In fact, we have that the roots of the characteristic equation (34) are in module all less than 1 (this guarantees that the numerical scheme is stable) if the following conditions are satisfied

- $p(1)\ge 0$, which is trivially verified since $\Gamma\le 0$;
- $(-1)^3p(-1)>0\Leftrightarrow p(-1)<0$, if the restriction

$$\tau_{q_1}\Gamma(\Delta t)^3+2(\tau_{q_1}+\tau_{q_2}Z)(\tau_d-\tau_{q_1}\Gamma)(\Delta t)^2-8\tau_d(\tau_{q_1}+\tau_{q_2}Z)^2\Delta t+8\tau_d(\tau_{q_1}+\tau_{q_2}Z)^3>0$$

holds;
- $|a_3|>|a_0|$, which is satisfied if the inequality

$$0<\tilde{a}_0<2a_3,$$

with

$$\tilde{a}_0=2\frac{\tau_d(\tau_{q_1}+\tau_{q_2}Z)^2}{\tau_{q_1}(\Delta t)^2}-\frac{\tau_{q_1}+\tau_{q_2}Z}{\Delta t}\left(\frac{\tau_d}{\tau_{q_1}}-\Gamma\right)-\Gamma$$

is guaranteed;
- $|b_2|<|b_0|$, wherein:

$$b_2=\begin{vmatrix}a_0 & a_1\\ a_3 & a_2\end{vmatrix},\quad b_0=\begin{vmatrix}a_0 & a_3\\ a_3 & a_0\end{vmatrix}.$$

This inequality can be rearranged into the form

$$|a_0a_2-a_1a_3|<|a_0^2-a_3^2|$$

which is fulfilled if the condition $-a_0^2-a_3^2<a_0a_2-a_1a_3<a_0^2+a_3^2$ holds.

After some calculation, constraints 1. and 2. are obtained from the above restrictions. □

In order to perform the numerical solutions, since the first condition of the theorem includes the term Γ, without losing its generality, after introducing its minimum value, $\min(\Gamma)$ obtained with positions $S_1=S_2=1$,

$$\min(\Gamma)=-2\left(\frac{\tau_{p_1}^{q_y}+\tau_{p_2}^{q_y}Z}{(\Delta y)^2}+\frac{\tau_{p_1}^{q_x}+\tau_{p_2}^{q_x}Z}{\hat{L}(\Delta x)^2}\right), \tag{36}$$

we impose the following stronger constraint for the time step Δt

$$\Delta t<-\frac{\tau_d(\tau_{q_1}+\tau_{q_2}Z)}{2\tau_{q_1}\min(\Gamma)}\le-\frac{\tau_d(\tau_{q_1}+\tau_{q_2}Z)}{2\tau_{q_1}\Gamma} \tag{37}$$

To proceed further, after substituting the value of $\min(\Gamma)$, expressed by (36), in the relation (37), after simple calculations the final form of the previous inequality reads

$$\Delta t<\frac{\tau_d}{4}\cdot\frac{\tau_{q_1}+\tau_{q_2}Z}{\tau_{q_1}}\cdot\frac{\hat{L}(\Delta x)^2(\Delta y)^2}{\hat{L}(\Delta x)^2\left(\tau_{p_1}^{q_y}+\tau_{p_2}^{q_y}Z\right)+(\Delta y)^2\left(\tau_{p_1}^{q_x}+\tau_{p_2}^{q_x}Z\right)} \tag{38}$$

Remark 3. It can be easily recognized that if

$$\tau_{p_1}^{q_y}=\tau_{p1}^{q_y}=0,\qquad \tau_{p1}^{q_x}=\tau_{p_1},\qquad \tau_{p_2}^{q_x}=\tau_{p_2},\qquad \hat{L}=1,\qquad \Delta x=\Delta y;$$

then

$$\Delta t<\frac{(\Delta x)^2}{4}\cdot\frac{\tau_{q_1}+\tau_{q_2}Z}{\tau_{q_1}}\cdot\frac{\tau_d}{\tau_{p_1}+\tau_{p_2}Z}, \tag{39}$$

and the one-dimensional situation of the CV heat equation is recovered, [29].

4. Numerical results

In this Section, we present some numerical solutions of the nonlinear CV heat equation, and the effects of nonlinear terms are discussed. Consider a domain with $L_1=L_2=7.9\cdot10^{-3}$ m. In detail, let us choose the present set of material parameters, such as the mass density $\rho_0=2866$

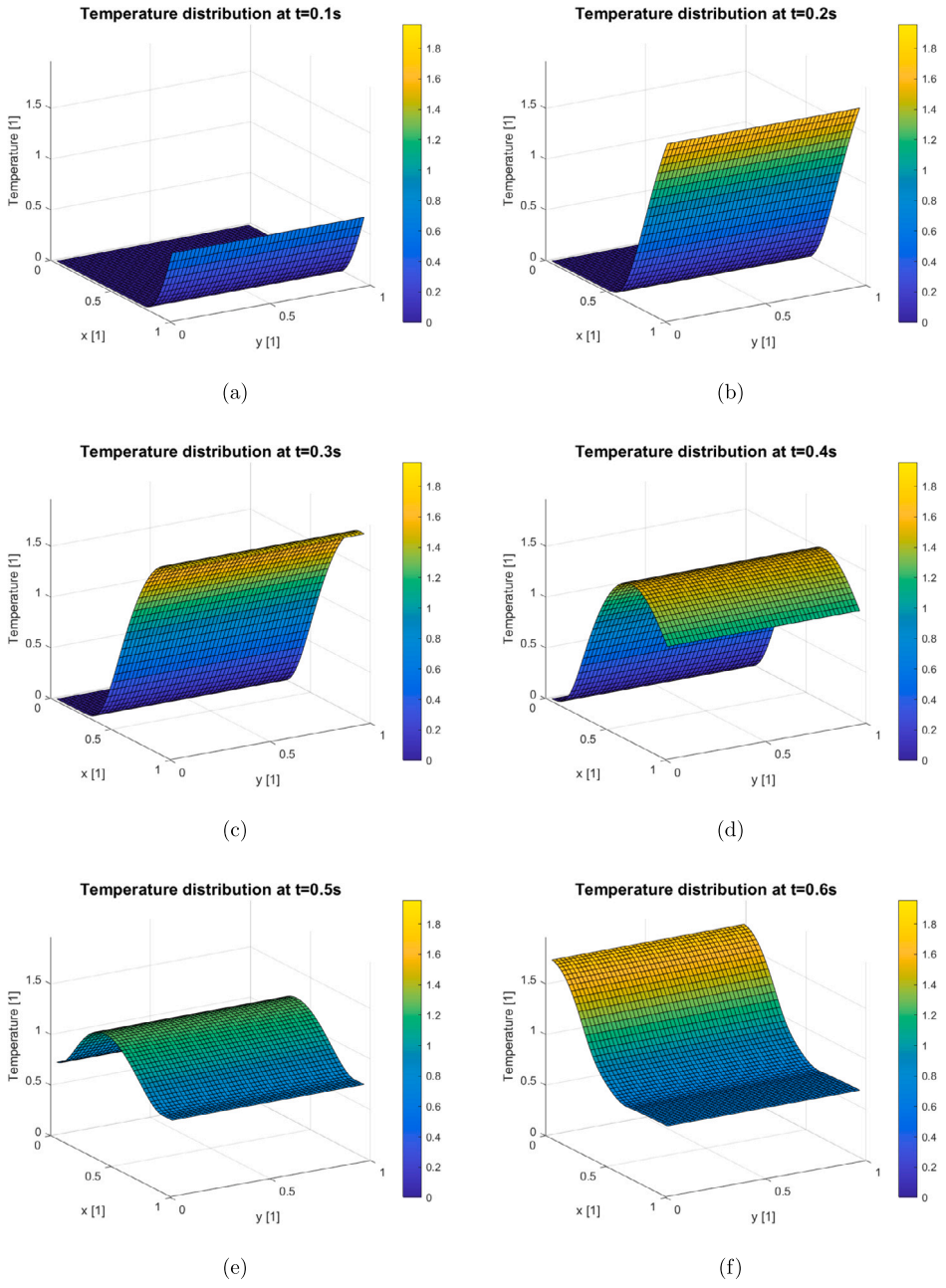

Fig. 4. Temperature distribution of the sample, for different time instants, using the boundary conditions homogeneous in space. (For interpretation of the colors in the figure(s), the reader is referred to the web version of this article.)

kg/m^3, the specific heat capacity $c = 1.81$ J/(kg K), the thermal conductivity $\lambda_0 = 150001$ W/(m K), and the relaxation time $\tau_0 = 3.8 \cdot 10^{-6}$ s. Then we obtain the following dimensionless parameters,

$$\tau_d = 0.4659, \quad \tau_{q_1} = 0.1770, \quad \tau_{q_2} = 0.01, \quad \tau_{p_1}^{q_x} = 0.4659,$$
$$\tau_{p_1}^{q_y} = 0.4659, \quad \tau_{p_2}^{q_x} = 0.03; \quad \tau_{p_2}^{q_y} = 0.02, \quad \hat{L} = 1.$$

Numerical integrations are performed by using the scheme (29a)-(29c) with the spatial and time steps $\Delta x = \Delta y = 0.02$ and $\Delta t = 10^{-5}$ respectively, where the complete time interval is $t_{max} = 2.6$ s. The initial conditions are expressed by (20) with the initial temperature $T_0 = 13$ K. As regards the boundary conditions are chosen in such a way that only one side of the square domain is non-adiabatic. In addition, these conditions are expressed by relations (21)-(22) in the case of spatially homogeneous heat pulse is assigned or by (21)-(23) in the spatially non-homogeneous case. In both cases, the numerical results are obtained using the pulse duration is $t_p = 1.0 \cdot 10^{-5}$ s and the maximum heat flux $q_{max} = 1.0 \cdot 10^4$ W/m^2.

The values of the temperature distribution have been represented by a color scale ranging from yellow (maximum value) to blue (minimum value).

Figs. 4 and 5 display the temperature distribution in the points of the domain in several time instants.

It can be observed that the heat pulse assigned to the edge leads to the same value at every point of the non-adiabatic edge. In case it has a higher intensity in the center, there is a gradual decrease going towards the boundary propagating in the y direction. A damping follows this until it reaches the opposite side, which, being adiabatic, provides a reflection of the thermal pulse. These rebounds continue until the thermal perturbation is entirely damped and the system reaches its equilibrium value, which, in the dimensionless case is equal to 1 (see Figs. 6(a) and 6(b)).

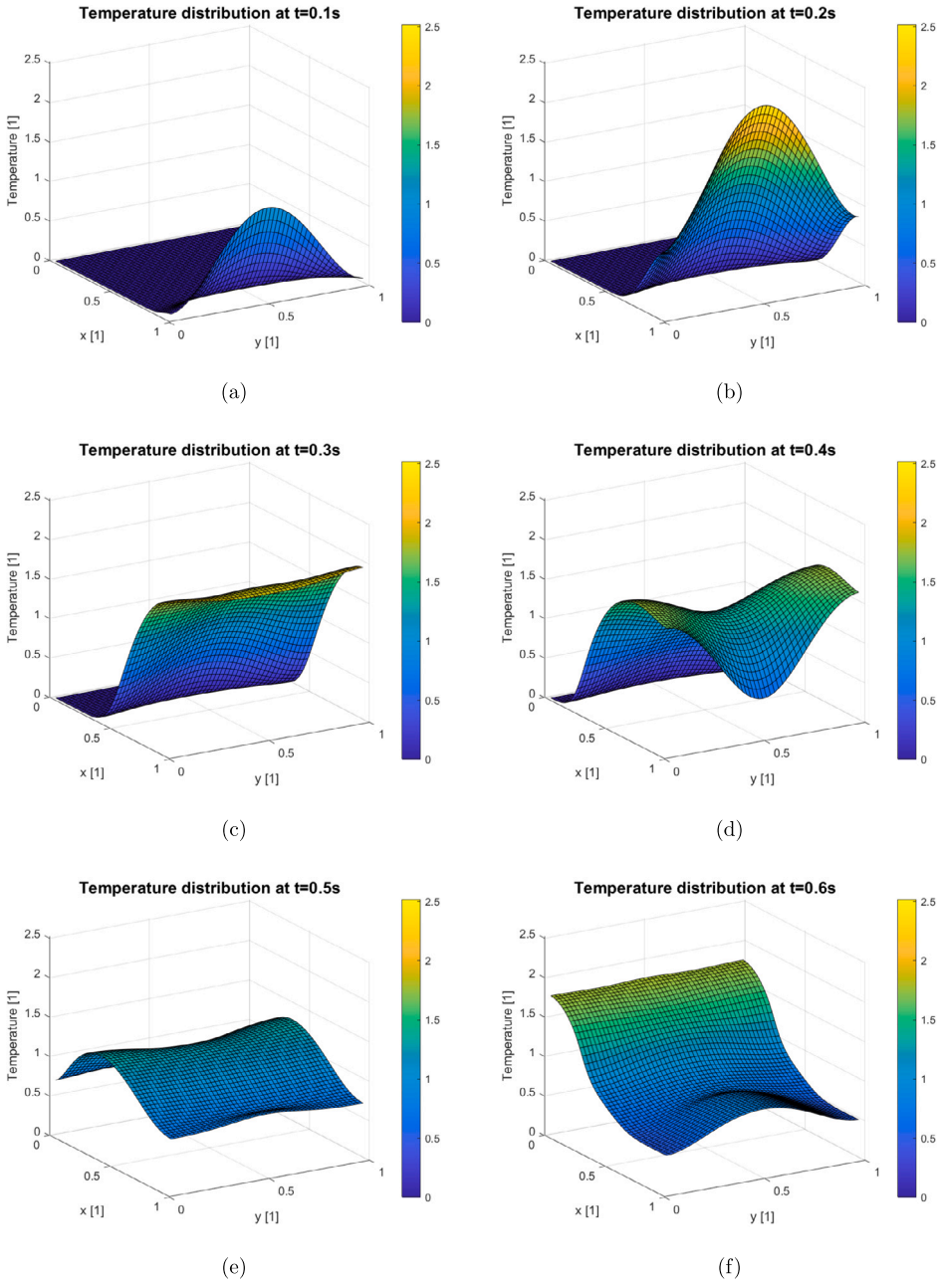

Fig. 5. Temperature distribution of the sample, for different time instants, using the boundary conditions non-homogeneous in space.

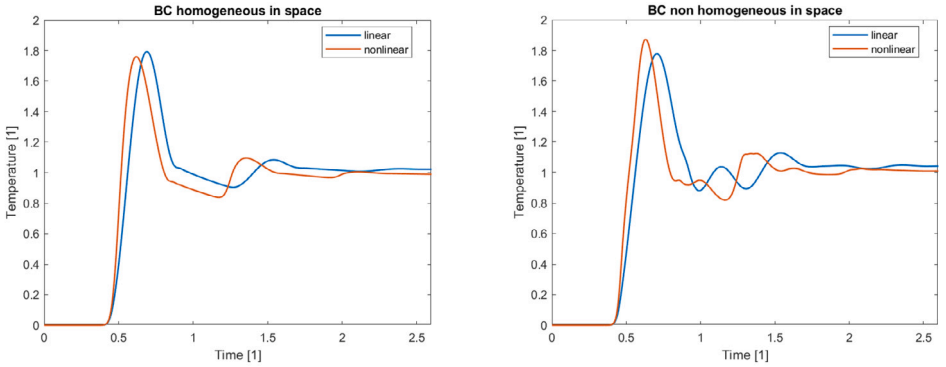

(a) (b)

Fig. 6. Comparison between linear and nonlinear solution, with (a) boundary conditions homogeneous in space, (b) boundary conditions non-homogeneous in space.

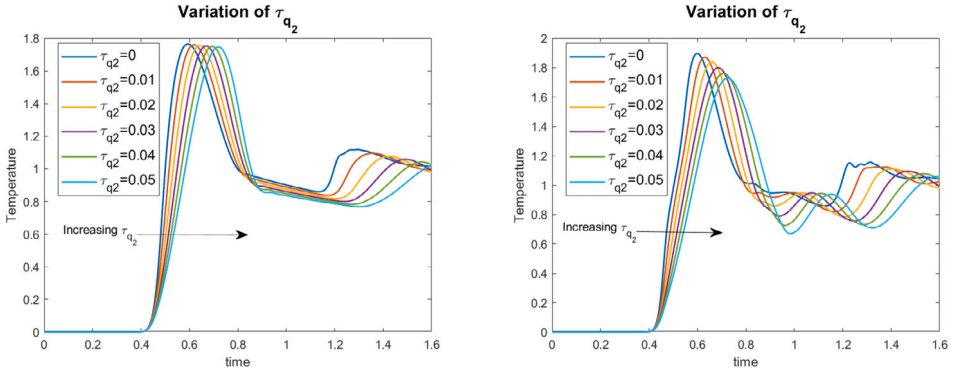

(a) (b)

Fig. 7. The temperature history when increasing the nonlinear parameter $\tau_{q_2} \in \{0, 0.01, 0.02, 0.03, 0.04, 0.05\}$ in (a) homogeneous boundary conditions and (b) non-homogeneous boundary conditions). Other parameters are: $\tau_d = 0.4659$, $\tau_{q_1} = 0.1770$, $\tau_{p_1}^{q_x} = 0.4659$, $\tau_{p_2}^{q_x} = 0.3$, $\tau_{p_1}^{q_y} = 0.4659$, $\tau_{p_2}^{q_y} = 0.2$ and $\hat{L} = 1$.

Comparing the linear problem (24a)-(24c) with the nonlinear one (19a)-(19c), we can deduce that the presence of nonlinearities in thermal conductivity and relaxation time (11a) and (11b) involves a delay in the propagation of the thermal signal.

The effects of nonlinear terms have been studied in more detail. Seemingly, the parameters, τ_{q_2} and $\tau_{p_2}^{q_y}$, act oppositely. In particular, their increase affects the slope when the temperature increases, implying a signal significantly shifted to the right or left. In fact, it is observed that increasing the value of the parameter τ_{q_2}, the wave signal is shifted to the right, this occurs independently of the type of boundary conditions assigned (either in the homogeneous case (see Fig. 7(a)) or in the non-homogeneous case (see Fig. 7(b)). An opposite behavior is observed if the value of the parameter $\tau_{p_2}^{q_y}$ is increased, as it is emphasized in the Figs. 8(a) and 8(b).

It is worth pointing out the absence of variations in the signal varying another nonlinear parameter, $\tau_{p_2}^{q_x}$, (see Figs. 9(a) and 9(b)). However, in both situations, the solution remains stable, and the dispersive error can be reduced by increasing the resolution of the discretization.

Numerical stability, dissipative and dispersive errors are analyzed in detail in the Appendix A

5. Conclusions

In the present paper, we studied the two-dimensional CV equation's linear and nonlinear versions. We considered the linear temperature dependence of the thermal conductivity and relaxation time, with a simplification that we neglect the mechanical effects at this stage of research. We used a staggered numerical scheme for discretization, for which we proved its stability and convergence properties. We note that the method to estimate the stability limit by reducing the original nonlinear problem to a linear one can be helpful but still lacks the mathematical rigor to provide a more reliable a-priori estimation for the maximum value of the temperature field. Despite this, it helped us to run efficient simulations. Regarding the solutions, we studied temperature histories which could be measured in a heat pulse experiment. We found that changing both T-dependent material parameters can significantly modify the measurable temperature history. On the one hand, they affect the steepness of the wavefront, therefore, from an experimental point of view, that could be an immediate indicator of any nonlinearities. On the other hand, the parameters can result in opposite effects, making it more challenging to uniquely determine the exact nonlinearities observed in the measurement. Interestingly, in a two-dimensional situation with spatially non-homogeneous boundary conditions, there is a remarkable delay in the second rear-side reflection compared to the linear case. Stronger oscillations are present, too. These oscillations are not artificial, as we excluded that possibility by investigating the dispersion properties of the scheme. These attributes together can be helpful for future experimental studies.

It is also worth pointing out that, since the real heat transfer situations are associated with complex geometries, in future researches the analysis of nonlinear heat conduction could be extended to situations with irregular domains. Although the solution method is not restricted to the present case, it is indeed difficult to implement that method for complicated geometries. More complex geometries can also be solved by other numerical methods such as the finite element or finite volume method, [38]. However, it is also useful to mention that the finite element discretization of such problems is not straightforward. Previous analyses performed with COMSOL showed that even in a one-dimensional case, [35], COMSOL can lead to false solutions. Therefore, our aim is to first study the behavior of such nonlinear heat equation

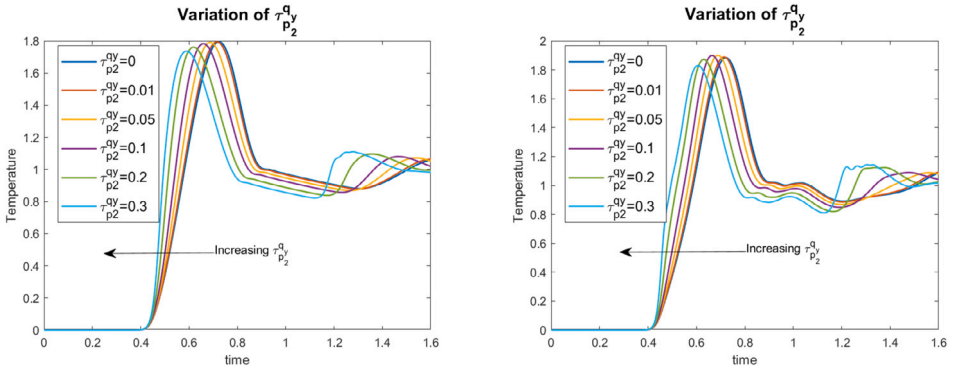

Fig. 8. The temperature history for increasing the nonlinear parameter $\tau_{p_2}^{q_y} \in \{0, 0.01, 0.05, 0.1, 0.2, 0.3\}$ in (a) homogeneous boundary conditions and (b) non-homogeneous boundary conditions). Other parameters are: $\tau_d = 0.4659$, $\tau_{q_1} = 0.1770$, $\tau_{q_2} = 0.01$, $\tau_{p_1}^{q_x} = 0.4659$, $\tau_{p_2}^{q_x} = 0.3$, $\tau_{p_1}^{q_y} = 0.4659$ and $\hat{L} = 1$.

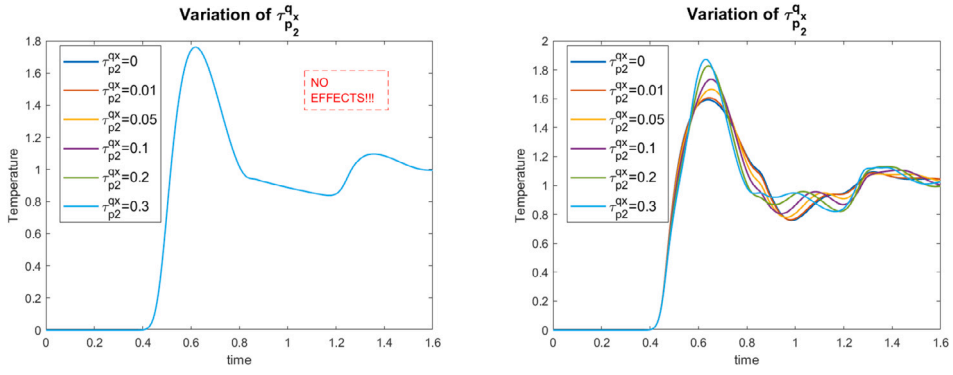

Fig. 9. The temperature history when increasing the nonlinear parameter $\tau_{p_2}^{q_x} \in \{0, 0.01, 0.05, 0.1, 0.2, 0.3\}$ in (a) homogeneous boundary conditions and (b) non-homogeneous boundary conditions). Other parameters are: $\tau_d = 0.4659$, $\tau_{q_1} = 0.1770$, $\tau_{q_2} = 0.01$, $\tau_{p_1}^{q_x} = 0.4659$, $\tau_{p_1}^{q_y} = 0.4659$, $\tau_{p_2}^{q_y} = 0.2$ and $\hat{L} = 1$.

with a thorough numerical analyses, and it is our future plan to extend our results to more complicated problems.

CRediT authorship contribution statement

C.F. Munafò: Conceptualization, Formal analysis, Investigation, Methodology, Software, Supervision, Validation, Visualization, Writing – original draft, Writing – review & editing. **P. Rogolino:** Conceptualization, Formal analysis, Investigation, Methodology, Supervision, Visualization, Writing – original draft, Writing – review & editing. **R. Kovács:** Conceptualization, Formal analysis, Investigation, Methodology, Software, Supervision, Validation, Visualization, Writing – original draft, Writing – review & editing.

Declaration of competing interest

The authors declare that they have no known competing financial interests or personal relationships that could have appeared to influence the work reported in this paper.

Data availability

No data was used for the research described in the article.

Acknowledgements

C.F.M. thanks GNFM–INdAM (Istituto Nazionale di Alta Matematica) for financial support through the grant 'Progetto Giovani' CUP-E53C22001930001. P.R. acknowledges the support of GNFM–INdAM (Istituto Nazionale di Alta Matematica).

Project no. TKP-6-6/PALY-2021 has been implemented with the support provided by the Ministry of Culture and Innovation of Hungary from the National Research, Development and Innovation Fund, financed under the TKP2021-NVA funding scheme. The research was funded by the grant National Research, Development and Innovation Office-NKFIH FK 134277, and also supported by the János Bolyai Research Scholarship of the Hungarian Academy of Sciences (RK).

Appendix A. Dissipation and dispersion errors of two-dimensional nonlinear CV model

The investigation of the dissipation (artificial decrease of the amplitude) and dispersion errors (artificial oscillations) is an important task as the simulation outcomes can be significantly distorted by these errors.

As it is possible to see from the Fig. A.11, using non-homogeneous boundary conditions the solution is affected by more evident oscillations. In both situations the significant oscillations highlighted in the Figs. A.10 (c)-(d) and A.11 (c)-(d) leading to the instability of the solution are the consequence of the fact that the time step is higher than the threshold value of time step that guarantees the stability of the solution.

More insight is provided by Figs. A.12, A.13, A.14 and A.15.

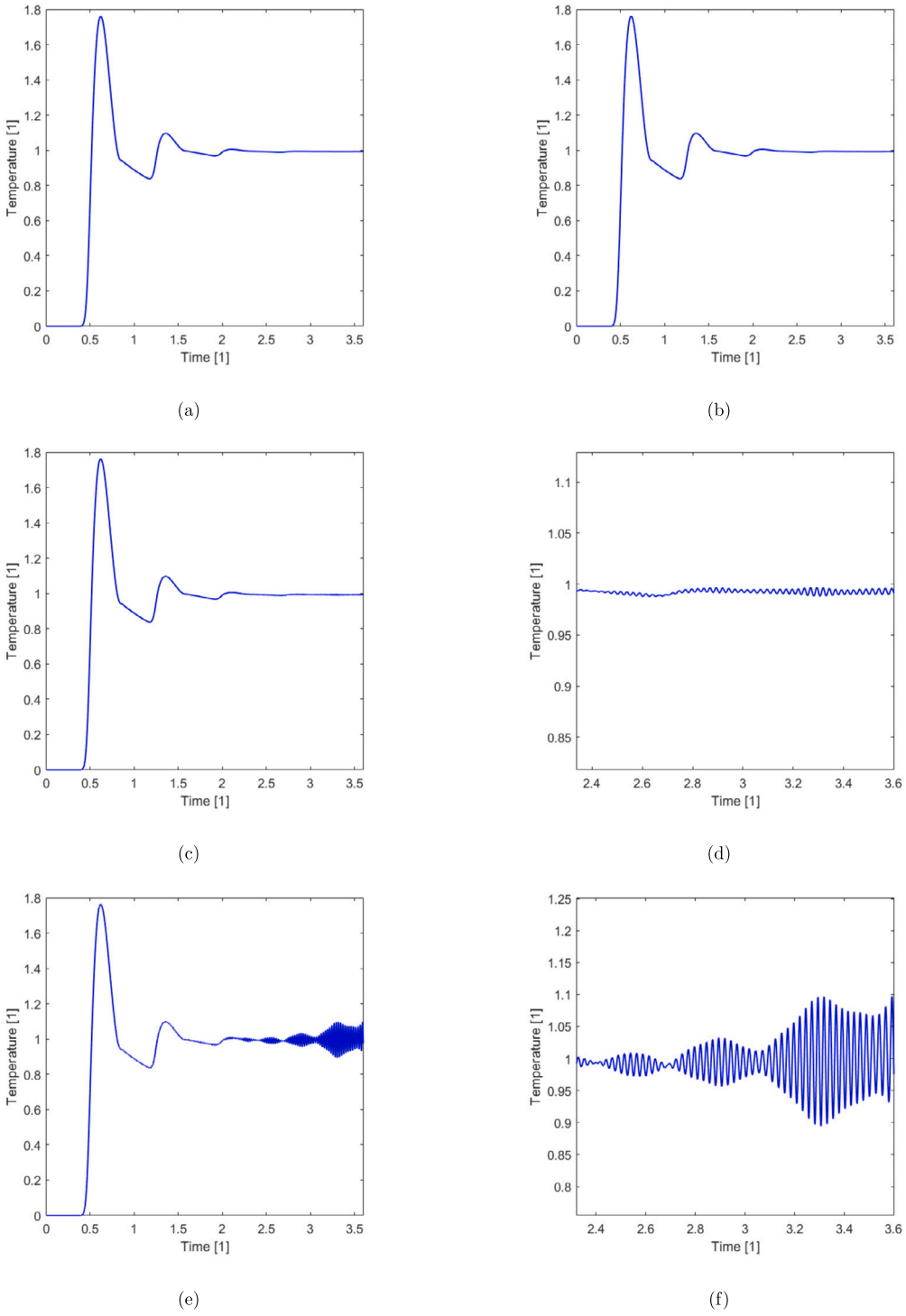

Fig. A.10. Homogeneous boundary conditions in space, $\Delta x = \Delta y = 0.02, \Delta t_{min} = 5.0367 \cdot 10^{-5}$ (a) $\Delta t = 10^{-5}$, (b) $\Delta t = \Delta t_{min}$, (c)-(d) $\Delta t = 1.2 \cdot 10^{-4}$ and (e)-(f) $\Delta t = 1.5 \cdot 10^{-4}$.

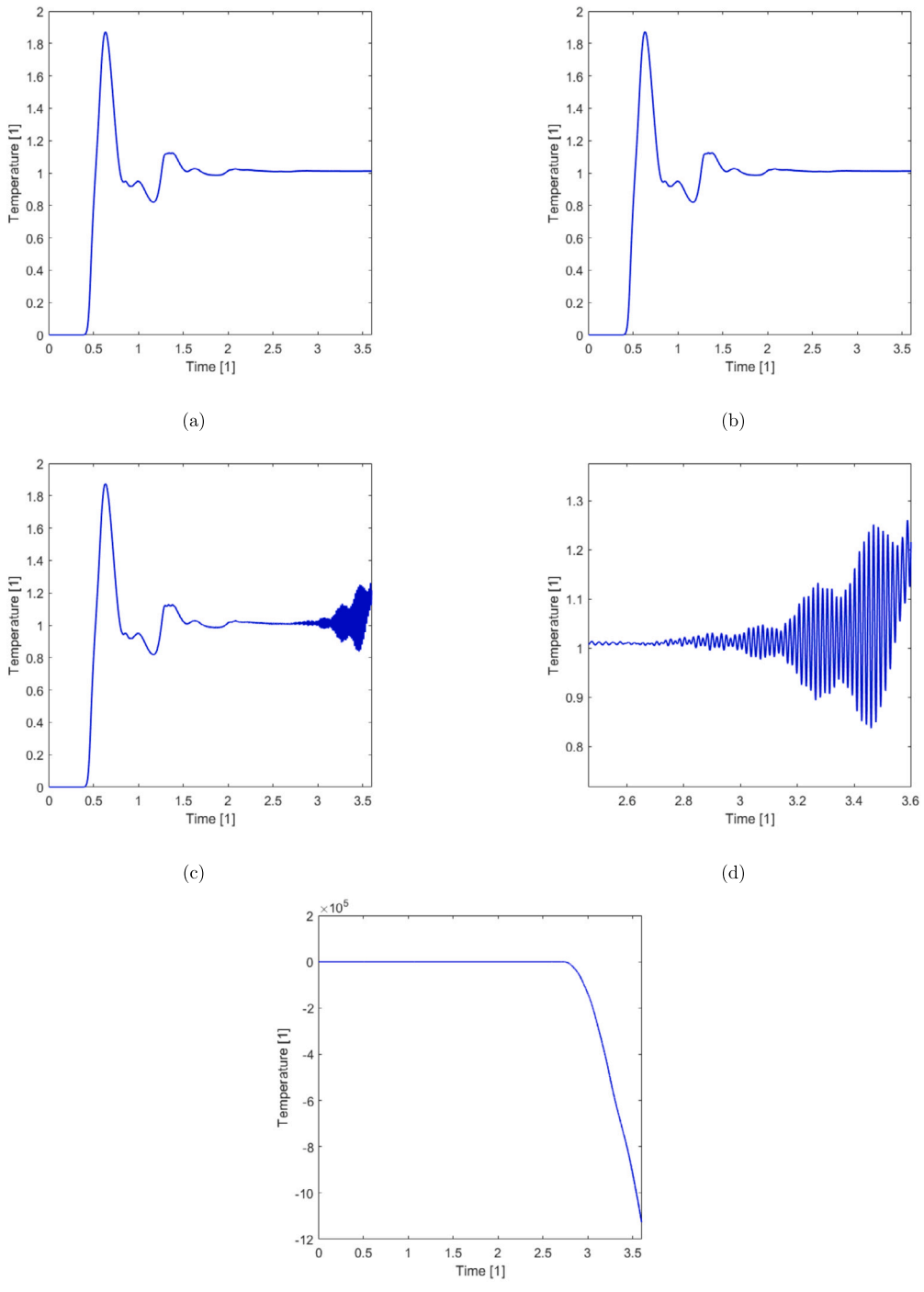

Fig. A.11. Non-homogeneous boundary conditions in space, $\Delta x = \Delta y = 0.02, \Delta t_{min} = 5.0367 \cdot 10^{-5}$ (a) $\Delta t = 10^{-5}$, (b) $\Delta t = \Delta t_{min}$, (c)-(d) $\Delta t = 1.2 \cdot 10^{-4}$ and (e) $\Delta t = 1.5 \cdot 10^{-4}$.

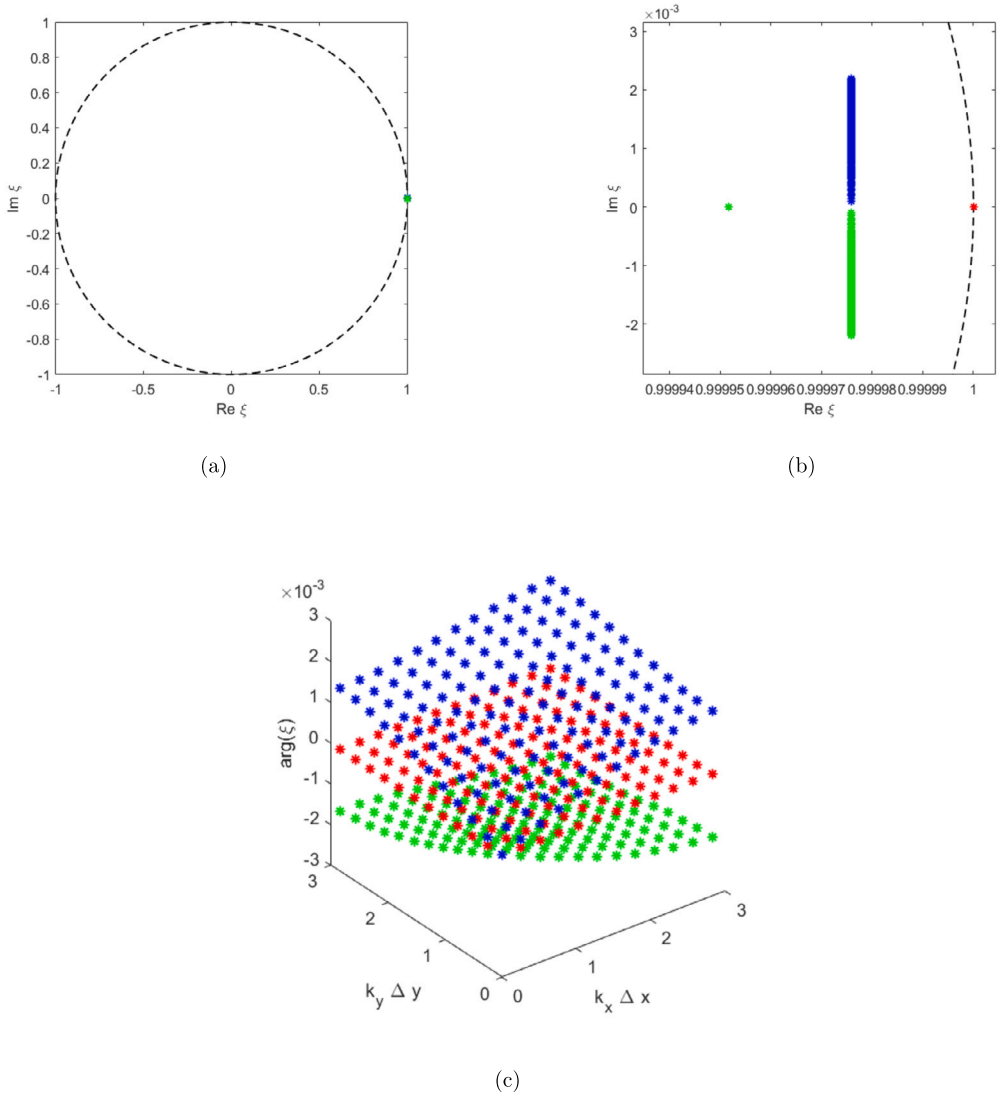

Fig. A.12. (a)-(b) The roots of $p(\xi)$ and (c) their argument, with $\Delta x = \Delta y = 0.02, \Delta t = 10^{-5} \leq \Delta t_{min} = 5.0367 \cdot 10^{-5}$. The maximum is chosen $Z = 3$. The maximum of the modulus of each roots is: $\max |\xi_1| = 1.00000, \max |\xi_2| = 0.99998, \max |\xi_3| = 0.99998$.

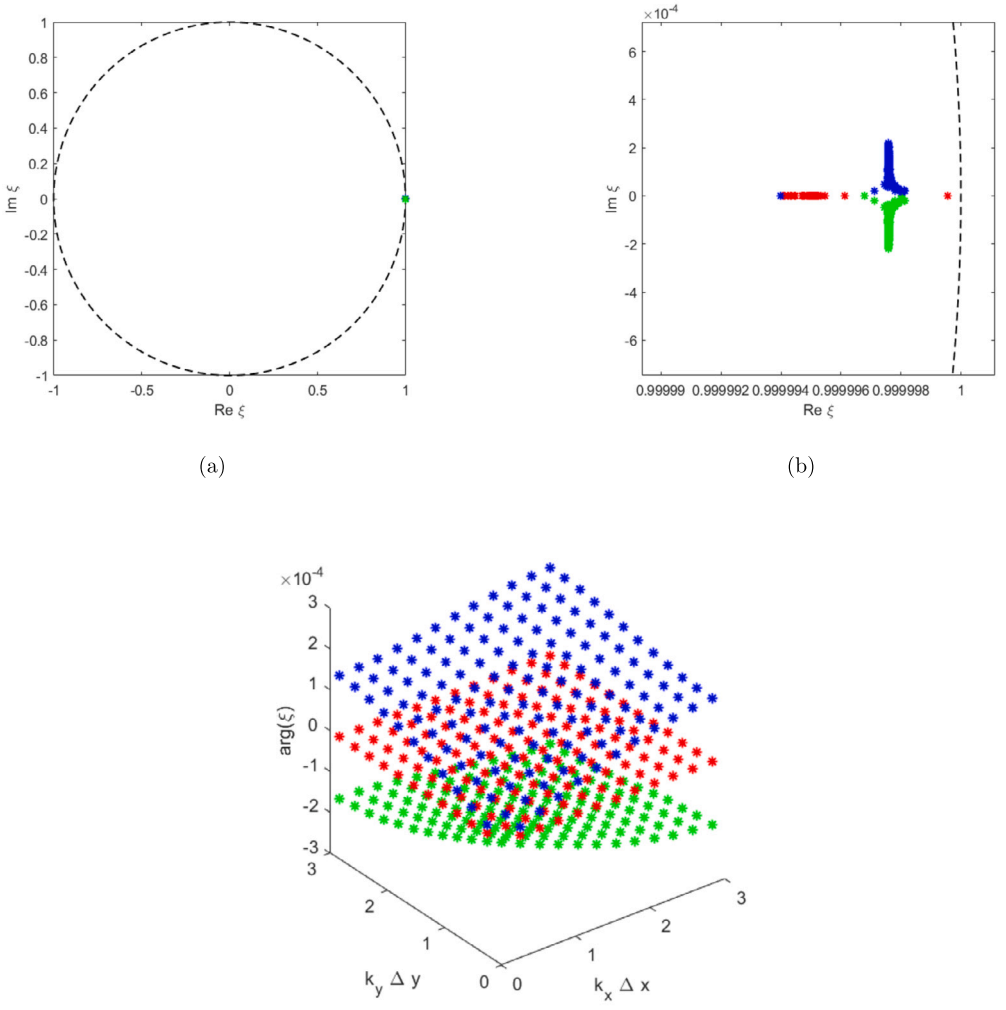

(a) (b) (c)

Fig. A.13. (a)-(b) The roots of $p(\xi)$ and (c) their argument, with $\Delta x = \Delta y = 0.02, \Delta t = 10^{-6} \leq \Delta t_{min} = 5.0367 \cdot 10^{-5}$. The maximum is chosen $Z = 3$. The maximum of the modulus of each roots is: $\max |\xi_1| = 1.00000, \max |\xi_2| = 1.00000, \max |\xi_3| = 1.00000$.

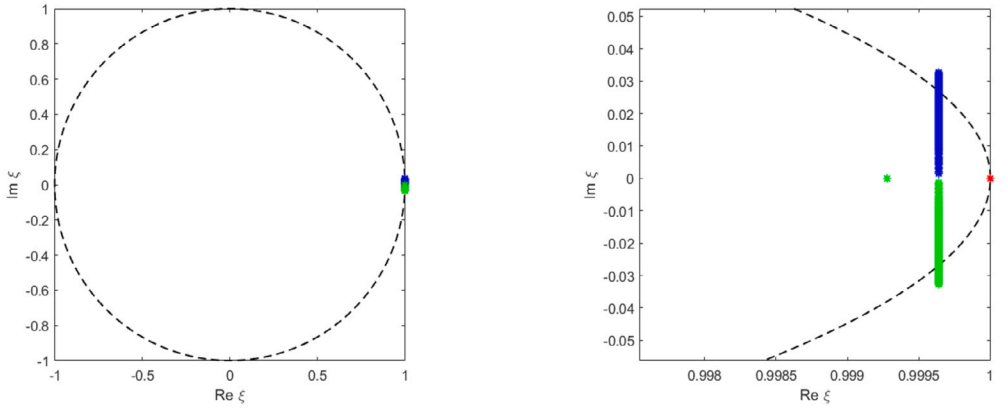

(a) (b)

Fig. A.14. The roots of $p(\xi)$ with $\Delta x = \Delta y = 0.02, \Delta t = 1.5 \cdot 10^{-4} \geq \Delta t_{min} = 5.0367 \cdot 10^{-5}$. The maximum is chosen $Z = 3$. The maximum of the modulus of each roots is: $\max |\xi_1| = 1.0000, \max |\xi_2| = 1.00018, \max |\xi_3| = 1.00018$.

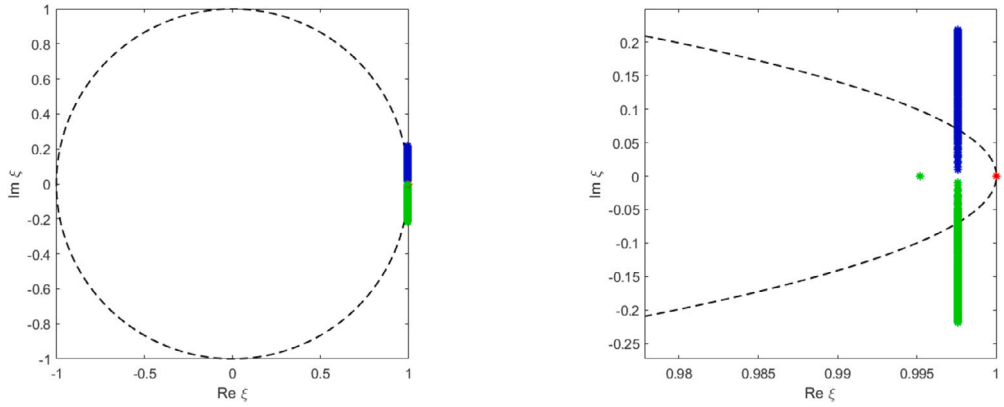

(a) (b)

Fig. A.15. The roots of $p(\xi)$ with $\Delta x = \Delta y = 0.02, \Delta t = 10^{-3} \geq \Delta t_{min} = 5.0367 \cdot 10^{-5}$. The maximum is chosen $Z = 3$. The maximum of the modulus of each roots is: $\max|\xi_1| = 1.0000, \max|\xi_2| = 1.02131, \max|\xi_3| = 1.02131$.

Appendix B. Stability, dissipation and dispersion errors of the one-dimensional nonlinear CV model

Here we recall some results presented in [29] with the aim of investigating the dispersion and dissipation errors in the case of the one-dimensional nonlinear CV heat equation. The characteristic equation for ξ ($\det \mathbf{M} = 0$) can be expressed as

$$p(\xi) = a_2\xi^2 + a_1\xi + a_0 = 0, \tag{B.1}$$

for which the coefficients are the following:

$$a_2 = \frac{\tau_{p_1}(\tau_{q_1} + \tau_{q_2}Z)^2}{\tau_{q_1}(\Delta t)^2}, \tag{B.2a}$$

$$a_1 = -2\frac{\tau_{p_1}(\tau_{q_1} + \tau_{q_2}Z)^2}{\tau_{q_1}(\Delta t)^2} + \frac{\tau_{p_1}(\tau_{q_1} + \tau_{q_2}Z)}{\Delta t}, \tag{B.2b}$$

$$\begin{aligned} a_0 &= \frac{\tau_{p_1}(\tau_{q_1} + \tau_{q_2}Z)^2}{\tau_{q_1}(\Delta t)^2} - \frac{\tau_{p_1}(\tau_{q_1} + \tau_{q_2}Z)}{\Delta t} + \frac{2(\tau_{p_1} + \tau_{p_2}Z)}{(\Delta x)^2}\left[\cos(k_x\Delta_x) - 1\right] \\ &= \frac{\tau_{p_1}(\tau_{q_1} + \tau_{q_2}Z)^2}{\tau_{q_1}(\Delta t)^2} - \frac{\tau_{p_1}(\tau_{q_1} + \tau_{q_2}Z)}{\Delta t} - \frac{2(\tau_{p_1} + \tau_{p_2}Z)}{(\Delta x)^2}S^2, \end{aligned} \tag{B.2c}$$

with $S = \sin(k\Delta x/2)$.

Theorem 2. *The numerical scheme is stable if the following conditions are satisfied*

1. $\Delta t < 2(\tau_{q_1} + \tau_{q_2}Z)$,
2. $\Delta t < \dfrac{(\Delta x)^2}{4} \cdot \dfrac{\tau_{q_1} + \tau_{q_2}Z}{\tau_{q_1}} \cdot \dfrac{\tau_{p_1}}{\tau_{p_1} + \tau_{p_2}Z}$.

Proof. For details, see [29]. □

Similarly to the two-dimensional case, the analysis of the dissipation and dispersion errors is shown in the Figs. B.16, B.17, B.18, B.19.

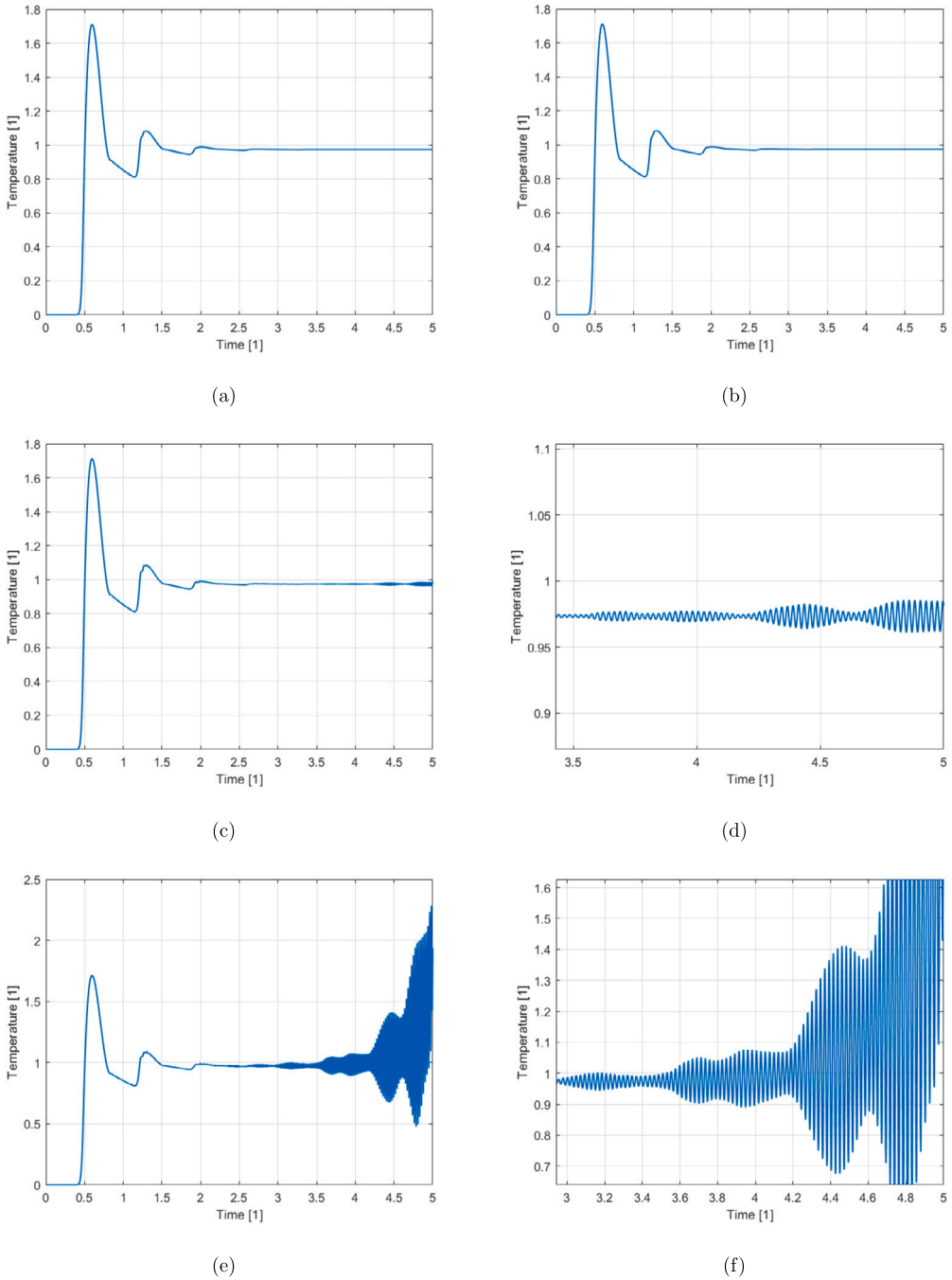

Fig. B.16. BC homogeneous in space, $\Delta x = 0.02, \Delta t_{min} = 9.8015 \cdot 10^{-5}$ (a) $\Delta t = 10^{-6}$, (b) $\Delta t = 10^{-5}$, (c)-(d) $\Delta t = \Delta t_{min}$ and (e)-(f) $\Delta t = 1.2 \cdot 10^{-4}$.

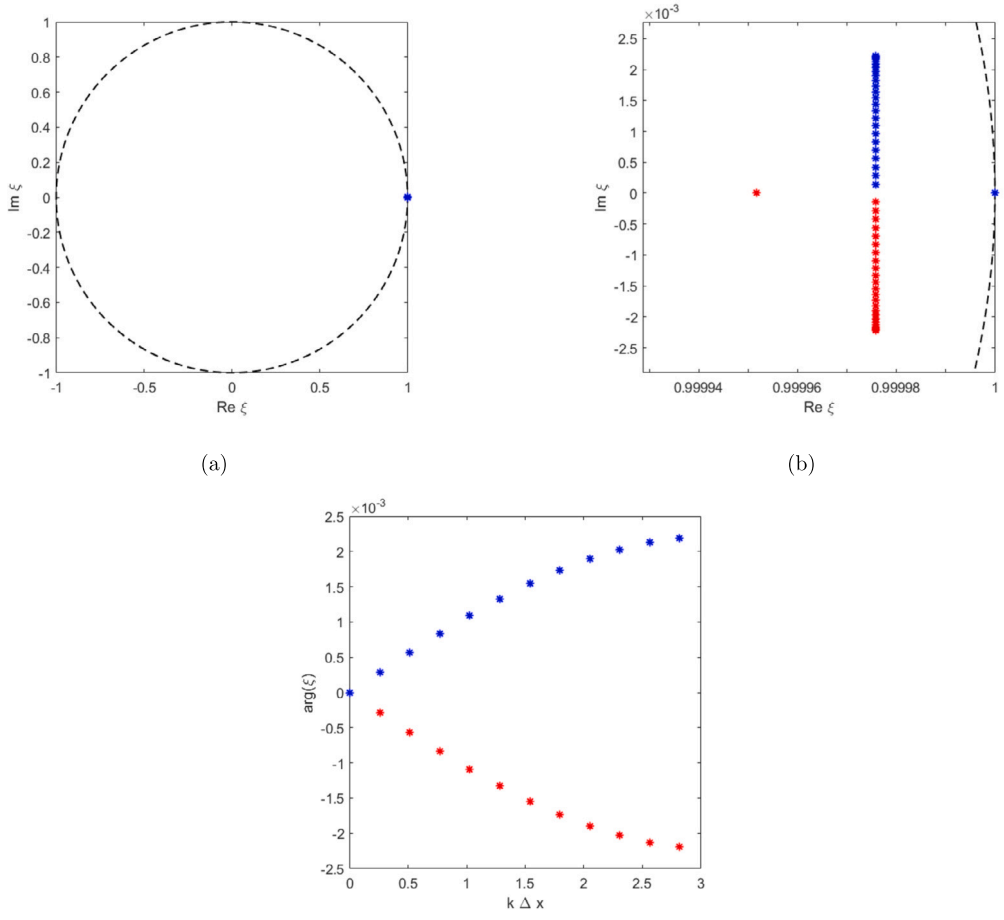

Fig. B.17. (a)-(b) The roots of $p(\xi)$ and (c) the argument, with $\Delta x = 0.02, \Delta t = 10^{-5} \leq \Delta t_{min} = 9.8015 \cdot 10^{-5}$. The maximum is chosen $Z = 3$. The maximum of the modulus of each roots is: $\max |\xi_1| = 1.00000, \max |\xi_2| = 1.00000$.

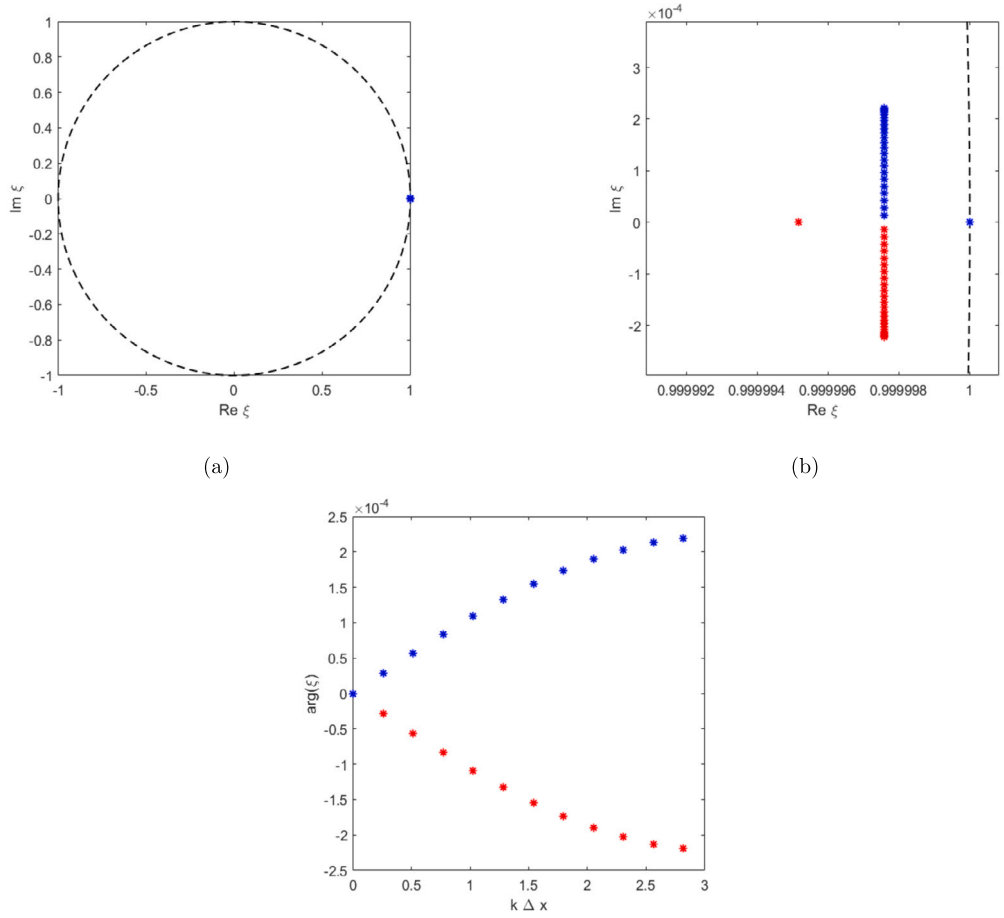

(a) (b) (c)

Fig. B.18. (a)-(b) The roots of $p(\xi)$ and (c) the argument, with $\Delta x = 0.02, \Delta t = 10^{-6} \leq \Delta t_{min} = 9.8015 \cdot 10^{-5}$. The maximum is chosen $Z = 3$. The maximum of the modulus of each roots is: $\max |\xi_1| = 1.00000, \max |\xi_2| = 1.00000$.

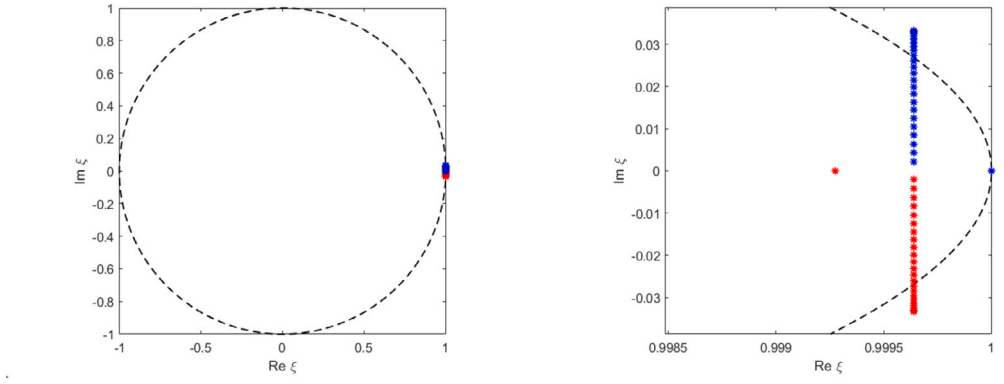

(a) (b)

Fig. B.19. (a)-(b) The roots of $p(\xi)$ and (c) the argument, with $\Delta x = 0.02, \Delta t = 1.5 \cdot 10^{-4} \geq \Delta t_{min} = 9.8015 \cdot 10^{-5}$. The maximum is chosen $Z = 3$. The maximum of the modulus of each roots is: $\max |\xi_1| = 1.00019, \max |\xi_2| = 1.00019$.

Appendix C. Accuracy order of nonlinear model

It is possible to estimate the accuracy order of the numerical scheme (in powers of $\Delta x, \Delta y$ and Δt). The error of the prediction for $(q_x)^{n+1}_{i+1/2,j}$ reads

$$
\begin{aligned}
&(q_x)^{n+1}_{i+1/2,j} - q_x(x_j, y_{i+1/2}, t_{n+1}) = \left(\frac{\Delta t}{\tau_{q_1} + \tau_{q_2} T^n_{i+1/2,j+1/2}} - 1 \right) (q_x)^n_{i+1/2,j} \\
&\quad - \frac{\left(\tau^{q_x}_{p_1} + \tau^{q_x}_{p_2} T^n_{i+1/2,j+1/2} \right)}{\left(\tau_{q_1} + \tau_{q_2} T^n_{i+1/2,j+1/2} \right)} \cdot \frac{\Delta t}{\Delta x} \cdot \left(T^n_{i+1/2,j+1/2} - T^n_{i+1/2,j-1/2} \right) \\
&\quad - q_x(x_j, y_{i+1/2}, t_{n+1}) \\
&\simeq \left(\frac{\Delta t}{\tau_{q_1} + \tau_{q_2} T(x_{j+1/2}, x_{i+1/2}, t_n)} - 1 \right) q_x(x_j, y_{i+1/2}, t_n) \\
&\quad - q_x(x_j, y_{i+1/2}, t_{n+1}) - \frac{\left(\tau^{q_x}_{p_1} + \tau^{q_x}_{p_2} T^n_{i+1/2,j+1/2} \right)}{\left(\tau_{q_1} + \tau_{q_2} T(x_{j+1/2}, x_{i+1/2}, t_n) \right)} \\
&\quad \cdot \frac{\Delta t}{\Delta x} \cdot \left[T(x_{j+1/2}, y_{i+1/2}, t_n) - T(x_{j-1/2}, x_{i+1/2}, t_n) \right] \\
&= - \left[q_x(x_j, y_{i+1/2}, t_{n+1}) - q_x(x_j, y_{i+1/2}, t_n) \right] \\
&\quad + \Delta t \cdot \frac{q_x(x_j, y_{i+1/2}, t_n)}{\tau_{q_1} + \tau_{q_2} T(x_{j+1/2}, x_{i+1/2}, t_n)} - \frac{\left(\tau^{q_x}_{p_1} + \tau^{q_x}_{p_2} T^n_{i+1/2,j+1/2} \right)}{\left(\tau_{q_1} + \tau_{q_2} T(x_{j+1/2}, x_{i+1/2}, t_n) \right)} \\
&\quad \cdot \frac{\Delta t}{\Delta x} \cdot \left[T(x_{j+1/2}, y_{i+1/2}, t_n) - T(x_{j-1/2}, x_{i+1/2}, t_n) \right] \\
&= -\Delta t \cdot \frac{\partial q_x}{\partial t}(x_j, y_{i+1/2}, t_n) + o(\Delta t^2) + \Delta t \cdot \frac{q_x(x_j, y_{i+1/2}, t_n)}{\tau_{q_1} + \tau_{q_2} T(x_{j+1/2}, x_{i+1/2}, t_n)} \\
&\quad - \frac{\left(\tau^{q_x}_{p_1} + \tau^{q_x}_{p_2} T^n_{i+1/2,j+1/2} \right)}{\left(\tau_{q_1} + \tau_{q_2} T(x_{j+1/2}, x_{i+1/2}, t_n) \right)} \cdot \frac{\Delta t}{\Delta x} \cdot \left[\Delta x \cdot \frac{\partial T}{\partial x}(x_j, x_{i+1/2}, t_n) + o(\Delta x^3) \right] \\
&= o(\Delta t^2) + o(\Delta x^2),
\end{aligned}
$$

after Taylor series expansion, simplification, and use of equation (19b). Analogously, after executing the same calculations, for the second component of heat flux we obtain

$$
(q_y)^{n+1}_{i,j+1/2} - q_y(x_{j+1/2}, y_i, t_{n+1}) = o(\Delta t^2) + o(\Delta y^2).
$$

The error of the prediction for $T^{n+1}_{i+1/2,j+1/2}$ is expressed as

$$
\begin{aligned}
&T^{n+1}_{i+1/2,j+1/2} - T(x_{j+1/2}, y_{i+1/2}, t_{n+1}) = T^n_{i+1/2,j+1/2} \\
&\quad - \hat{L} \frac{\left[(q_x)^n_{i+1/2,j+1} - (q_x)^n_{i+1/2,j} \right]}{\tau_d \left(1 + \frac{\tau_{q_2}}{\tau_{q_1}} T^n_{i+1/2,j+1/2} \right)} \cdot \frac{\Delta t}{\Delta x} - \frac{\left[(q_y)^n_{i+1,j+1/2} - (q_y)^n_{i,j+1/2} \right]}{\tau_d \left(1 + \frac{\tau_{q_2}}{\tau_{q_1}} T^n_{i+1/2,j+1/2} \right)} \cdot \frac{\Delta t}{\Delta y} \\
&\quad - T(x_{j+1/2}, y_{i+1/2}, t_{n+1}) \\
&\simeq - \left[T(x_{j+1/2}, y_{i+1/2}, t_{n+1}) - T(x_{j+1/2}, y_{i+1/2}, t_n) \right] \\
&\quad - \hat{L} \frac{\left[q_x(x_{j+1}, y_{i+1/2}, t_n) - q_x(x_j, y_{i+1/2}, t_n) \right]}{\tau_d \left(1 + \frac{\tau_{q_2}}{\tau_{q_1}} (x_{j+1/2}, y_{i+1/2}, t_n) \right)} \cdot \frac{\Delta t}{\Delta x} \\
&\quad - \frac{\left[q_y(x_{j+1/2}, y_{i+1}, t_n) - q_y(x_{j+1/2}, y_i, t_n) \right]}{\tau_d \left(1 + \frac{\tau_{q_2}}{\tau_{q_1}} T(x_{j+1/2}, y_{i+1/2}, t_n) \right)} \cdot \frac{\Delta t}{\Delta y} \\
&= -\Delta t \cdot \frac{\partial T}{\partial t}(x_{j+1/2}, y_{i+1/2}, t_n) + o(\Delta t^2) \\
&\quad - \frac{\hat{L}}{\tau_d \left(1 + \frac{\tau_{q_2}}{\tau_{q_1}} T^n_{i+1/2,j+1/2} \right)} \cdot \frac{\Delta t}{\Delta x} \cdot \left[\frac{\partial q_x}{\partial x}(x_j, y_{i+1/2}, t_n) \Delta x + o(\Delta x^2) \right] \\
&\quad - \frac{1}{\tau_d \left(1 + \frac{\tau_{q_2}}{\tau_{q_1}} T^n_{i+1/2,j+1/2} \right)} \cdot \frac{\Delta t}{\Delta y} \cdot \left[\frac{\partial q_y}{\partial y}(x_{j+1/2}, y_i, t_n) \Delta y + o(\Delta y^2) \right] \\
&= o(\Delta t^2) + o(\Delta x) + o(\Delta y),
\end{aligned}
$$

after Taylor series expansion, cancellation and use of equation (19a). Finally

$$
\begin{aligned}
&T^{n+1}_{i+1/2,j+1/2} - T(x_{j+1/2}, y_{i+1/2}, t_{n+1}) = o(\Delta t^2) + o(\Delta x) + o(\Delta y), \\
&(q_x)^{n+1}_{i+1/2,j} - q_x(x_j, y_{i+1/2}, t_{n+1}) = o(\Delta t^2) + o(\Delta x^2), \\
&(q_y)^{n+1}_{i,j+1/2} - q_y(x_{j+1/2}, y_i, t_{n+1}) = o(\Delta t^2) + o(\Delta y^2),
\end{aligned}
\tag{C.1}
$$

hence is proved the numerical scheme is second order accurate in time and first order in space, globally it is of order one.

References

[1] B.R. Appleton, G.K. Cellar, Laser and Electron Beam Interactions with Solids, Elsevier Science, New York, 1982.
[2] P. Rogolino, V.A. Cimmelli, Thermal conductivity and enhanced thermoelectric efficiency of composition-graded Si_cGe_{1-c} alloys, Z. Angew. Math. Phys. 71 (3) (2020) 92.
[3] B. Straughan, Heat Waves, vol. 17, Springer, Berlin, 2011.
[4] H.E. Jackson, C.T. Walker, Thermal conductivity, second sound, and phonon-phonon interactions in NaF, Phys. Rev. B 3 (4) (1971) 1428–1439.
[5] V. Narayanamurti, R.D. Dynes, Observation of second sound in bismuth, Phys. Rev. Lett. 28 (22) (1972) 1461–1465.
[6] T.F. McNelly, S.J. Rogers, D.J. Channin, R.J. Rollefson, W.M. Gouban, G.E. Schmidt, J.A. Krumhansl, R.O. Pohl, Heat pulses in NaF: onset of second sound, Phys. Rev. Lett. 24 (3) (1970) 100–102.
[7] D.W. Pohl, V. Irniger, Observation of second sound in NaF by means of light scattering, Phys. Rev. Lett. 36 (9) (1976) 480–483.
[8] R.J. Hardy, S.S. Jawsal, Velocity of second sound in NaF, Phys. Rev. B 3 (12) (1971) 4385–4387.
[9] H.E. Jackson, C.T. Walker, C.T. McNelly, Second sound in NaF, Phys. Rev. Lett. 25 (1) (1970) 26–29.
[10] P. Ván, T. Fülöp, Grog Gy, A. Gyenis, J. Verhas, Experimental aspects of heat conduction beyond Fourier, in: Proc. 12th Joint European Thermodynamics Conference, Brescia, 2013, pp. 519–524.
[11] T. Fülöp, R. Kovács, A. Lovas, A. Rieth, T. Fodor, M. Szücs, P. Ván, G. Gróf, Emergence of non-Fourier hierarchies, Entropy 20 (11) (2018) 832-1–832-13.
[12] X. Wang, X. Xu, Thermoelastic wave induced by pulsed laser heating, Appl. Phys. A 73 (2001) 107–114.
[13] A.A. Balandin, Thermal properties of graphene and nanostructured carbon materials, Nat. Mater. 10 (8) (2011) 569–581.
[14] C. Cattaneo, Sulla conduzione del calore, Atti Semin. Mat. Fis. Univ. Modena 3 (1948) 83–101.
[15] V.A. Cimmelli, D. Jou, T. Ruggeri, P. Ván, Entropy principle and recent results in non-equilibrium theories, Entropy 16 (3) (2014) 1756–1807.
[16] D. Jou, J. Casas-Vázquez, G. Lebon, Extended irreversible thermodynamics, Rep. Prog. Phys. 51 (8) (1988) 1105.
[17] D. Jou, J. Casas-Vázquez, G. Lebon, Extended Irreversible Thermodynamics, vol. 16, 4th revised edition, Springer, Berlin, 2010.
[18] P. Rogolino, V.A. Cimmelli, Differential consequences of balance laws in extended irreversible thermodynamics of rigid heat conductors, Proc. R. Lond. A 475 (2019) 2227.
[19] I. Müller, T. Ruggeri, Rational Extended Thermodynamics, vol. 37, 2nd edition, Springer, New York, 2013.
[20] I. Gyarmati, On the wave approach of thermodynamics and some problems of non-linear theories, J. Non-Equilib. Thermodyn. 2 (1977) 233–260.
[21] V.A. Cimmelli, A. Sellitto, D. Jou, Nonlocal effects and second sound in a non-equilibrium steady state, Phys. Rev. B 79 (1) (2009) 014303.
[22] P. Ván, T. Fülöp, Universality in heat conduction theory: weakly nonlocal thermodynamics, Ann. Phys. 524 (8) (2012) 470–478.
[23] S. Both, B. Czél, T. Fülöp, G. Gróf, A. Gyenis, R. Kovács, P. Ván, J. Verhás, Deviation from the Fourier law in room-temperature heat pulse experiments, J. Non-Equilib. Thermodyn. 41 (1) (2016) 41–48.
[24] R. Kovács, P. Ván, Generalized heat conduction in heat pulse experiments, Int. J. Heat Mass Transf. 83 (2015) 613–620.
[25] S. Saedodina, M.J. Noroozi, D.D. Ganjib, Investigation of the effects of non-linear and non-homogeneous non-Fourier heat conduction equations on temperature distribution in a semi-infinite body, IJE Trans. C, Asp. 28 (12) (2015) 1802–1807.
[26] R. Spigler, More around Cattaneo equation to describe heat transfer processes, Math. Methods Appl. Sci. 43 (9) (2020) 5953–5962.
[27] R.I. Nuruddeen, Approximate analytical solution to the Cattaneo heat conduction model with various laser sources, J. Appl. Math. Comput. Mech. 21 (1) (2022) 67–78.

[28] S. Carillo, P.M. Jordan, On the propagation of temperature-rate waves and traveling waves in rigid conductors of the Graffi–Franchi–Straughan type, Math. Comput. Simul. 176 (2020) 120–133.
[29] R. Kovács, P. Rogolino, Numerical treatment of nonlinear Fourier and Maxwell-Cattaneo-Vernotte heat transport equations, Int. J. Heat Mass Transf. 150 (119281) (2020) 119281.
[30] B.D. Coleman, W. Noll, The thermodynamics of elastic materials with heat conduction and viscosity, Arch. Ration. Mech. Anal. 13 (1963) 167–178.
[31] D. Jou, J. Casas-Vázquez, G. Lebon, Extended irreversible thermodynamics of heat transport: a brief introduction, Proc. Est. Acad. Sci. 57 (2008) 3.
[32] L. Onsager, Reciprocal relations in irreversible processes, Phys. Rev. 37 (4) (1931) 405.
[33] T. Fülöp, R. Kovács, M. Szücs, M. Fawaier, Thermodynamical extension of a symplectic numerical scheme with half space and time shifts demonstrated on rheological waves in solids, Entropy 22 (2) (2020) 155.
[34] A. Pozsár, M. Szücs, R. Kovács, T. Fülöp, Four spacetime dimensional simulation of rheological waves in solids and the merits of thermodynamics, Entropy 22 (12) (2020) 1376.
[35] A. Rieth, R. Kovács, T. Fülöp, Implicit numerical schemes for generalized heat conduction equations, Int. J. Heat Mass Transf. 126 (2018) 1177–1182.
[36] W.H. Press, Numerical recipes, in: The Art of Scientific Computing, 3rd edition, Cambridge University Press, 2007.
[37] E.I. Jury, L. Stark, V.V. Krishann, Inners and Stability of Dynamic Systems, 1974.
[38] A. Quarteroni, S. Quarteroni, Numerical Models for Differential Problems, Springer, 2009.